The Statistics of Superdirective Beam Patterns

Andrea Trucco, *Senior Member, IEEE*

***Abstract*—Superdirective arrays have been extensively studied because of their considerable potential accompanied, unfortunately, by a high sensitivity to random errors that affect the responses and positions of array elements. However, the statistics of their actual beam pattern (BP) has never been systematically investigated. This paper shows that the Rician probability density function (PDF), sometimes adopted to study the impact of errors in conventional arrays, is a valid approximation for superdirective BP statistics only where some mathematical terms are negligible. The paper also shows that this is the case for all linear end-fire arrays considered. A similar study is proposed concerning the correlation between BP lobes, showing that for the superdirective arrays considered the lobes, especially non-adjacent ones, are almost independent. Furthermore, knowledge of the PDF of the actual BP allows one to define quantile BP functions, whose probability of being exceeded, at any point, is fixed. Combining the lobes' independence with quantile BP functions, an empirical equation for the probability that the entire actual BP will not exceed a quantile function over an interval larger than a given size is obtained. This new knowledge and these tools make it possible to devise new methods to design robust superdirective arrays via optimization goals with clearer and more relevant statistical meaning.**

***Index Terms*—Beamforming, superdirective arrays, robust superdirectivity, beam pattern statistics, random errors, correlation, quantile functions, Rician PDF.**

I. Introduction

IN DATA-INDEPENDENT beamforming [1], superdirectivity theory (also called supergain) is often used [2]–[5] when the array aperture is comparable to or less than the wavelength. In this condition, uniform and side-lobe reduction weighting windows produce very limited directivity.[1] To improve performance, superdirective techniques allow the synthesis of weighting windows that increase the directivity, for a given array layout, subject to specific constraints. Special advantages are predicted for linear arrays steered at end-fire (i.e., along the array baseline) because this particular pointing has a maximum (theoretical) directivity of N^2 (N being the number of sensors) [4], [6], [7]. As an example, Fig. 1(a) compares the BPs of an 8-element end-fire linear array, with an inter-element spacing of 0.3λ (λ being the wavelength), when uniform and superdirective weighting windows are used.

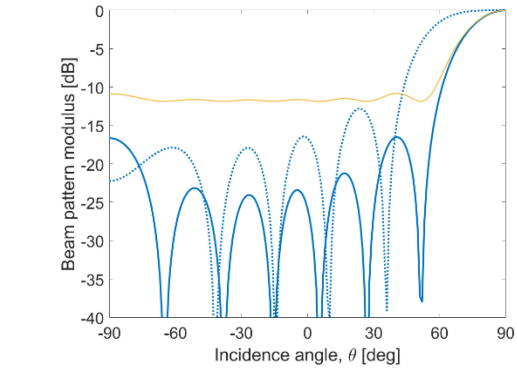

(a)

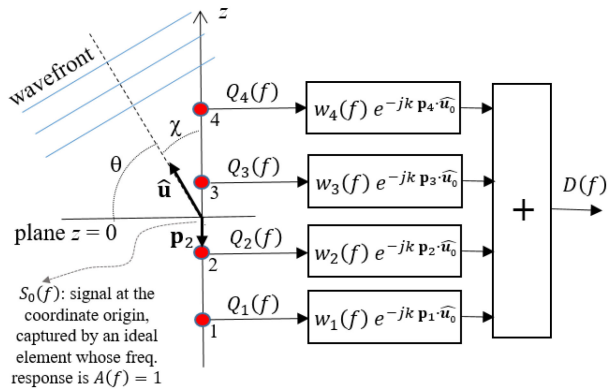

(b)

Fig. 1. (a) End-fire BPs for a linear array composed of 8 elements spaced 0.3λ, obtained with uniform (blue dotted line) and superdirective (blue solid line) weights. Mean value of the Rician PDF (golden line) for the modulus of the BP affected by random errors, for the C-4 case (see Section V). (b) Beamforming processing scheme with the adopted notation, for $N = 4$ (see Section II).

The possibility of considerably increasing the directivity makes superdirectivity a topic of great interest and current research [8]–[11], in view of numerous applications, including microphone array [12], [13], sonar [14], [15], radar [5], [16] and radio communication [6], [17]. The main research aim is to combine the increase in directivity with the reduction in robustness against spatially uncorrelated noise and random errors. Indeed, the nominal beam pattern (NBP, i.e., the one obtained in the absence of noise and errors) often differs significantly from the actual beam pattern (ABP, i.e., the one of a specific array realization, impacted by errors). To deal with this problem, many methods have been proposed to synthesize superdirective weighting windows capable of balancing an increased directivity with a sufficient robustness. Constrained optimization

Manuscript received September 28, 2021; revised January 26, 2022 and February 28, 2022; accepted March 1, 2022. Date of publication March 7, 2022; date of current version May 2, 2022. The associate editor coordinating the review of this manuscript and approving it for publication was Dr. Florian Roemer.

The author is with the Department of Electrical, Electronic, Telecommunications Engineering and Naval Architecture, University of Genoa, 16145 Genoa, Italy and also with the Pattern Analysis and Computer Vision Department, Istituto Italiano di Tecnologia (IIT), 16152 Genoa, Italy (e-mail: trucco@ieee.org).

Digital Object Identifier 10.1109/TSP.2022.3156700

[1]The directivity is the improvement in the signal-to-noise ratio obtained using the array instead of a single omnidirectional sensor, when an isotropic noise field and plane wave signal are considered.

techniques (maximizing the directivity subject to constraints on quantities related with the robustness to errors) have been proposed [1], [3]–[5], [12], as well as techniques that leverage the PDFs of random errors to optimize the expected beam power pattern (EBPP, i.e., the mean power of the ABP) or other statistical functions [18]–[22]. However, in the superdirectivity field, little attention has been paid to the complete characterization of the ABP, neglecting to deepen the knowledge of its PDF and to use it, on the one hand, to analyze the behavior of the superdirective array with respect to errors, on the other hand, to guide the optimization task.

The effect of random errors in data-independent beamforming with conventional arrays has been investigated for many decades [1], [5], [23]–[34], leading to equations for the calculation of the moments of the ABP (or of specific ABP portions, especially the side-lobe region) and, with different levels of approximation, to knowledge of the PDF of the ABP modulus. In many cases the studies are limited to gain and phase errors, considered constant with respect to frequency, neglecting errors in the positions of the array elements. Regarding the PDF of errors, previous studies have often been conducted exclusively for the Gaussian case or for the uniform case. Equally often, the analyses are exclusively referred to specific geometries, namely the equispaced linear or planar array. In this context, some authors [5], [23], [25], [26], [30], [31], [34] have shown that, under working conditions that are common for a conventional array, the PDF of the ABP modulus can be approximated by a Rician function. Furthermore, to calculate the probability that the side-lobe peak exceeds a given level, the Rician PDF was used assuming, in addition to the above-mentioned assumptions, the independence between the effects of random errors on different lobes [25], [26].

Unfortunately, the assumptions used in the past to show that the Rician PDF is a valid approximation for the statistics of the ABP modulus (in particular, real-valued weight coefficients, symmetric with respect to the array center [25], [30]) are not valid for superdirective arrays, where the weight coefficients are generally complex-valued and the white-noise gain (WNG)[2] markedly decreases. The first contribution of this paper is the analytical study of the terms that must be neglected for the ABP modulus to have Rician statistics, without introducing any constraints on the array geometry and comprising gain, phase and position errors for every sensor. In addition, the impact of the PDFs most commonly adopted to describe such errors is investigated. After identifying the equations of the terms that prevent the perfect "Ricianity" (equations valid for any kind of array), the paper shows that these terms are negligible for a number of linear end-fire arrays made superdirective through constrained optimization. The Ricianity of their ABPs is also verified with the Kolmogorov-Smirnov (KS) hypothesis test.

Knowledge of ABP modulus statistics allows this paper to introduce the quantile BP function, whose value, at a given arrival direction, will be exceeded by the ABP modulus with a known probability. Furthermore, the paper studies the independence between two points of the ABP, again without assumptions on the array geometry and without neglecting any of the error types already considered. The solutions of the mathematical expectations obtained assuming Gaussian spherical symmetry in position errors are applied to the linear superdirective arrays mentioned above, showing that the lobes of their ABPs are almost independent, especially non-adjacent ones. Finally, the relative frequency with which the ABP exceeds a quantile BP function, as a function of the size (in terms of angular interval) of the overrun, is analyzed using an empirical approach. Combining the outcomes of this analysis with the independence between lobes, a simple equation is proposed to approximate the probability that no overrun of the quantile BP function occurs with a size greater than a given value. The validity of this equation is assessed through numerical experimentation.

As described above, this paper introduces new knowledge regarding the statistics of BPs that characterize superdirective arrays. The importance of this new knowledge is twofold. On the one hand, mathematical tools are provided to test whether the Ricianity assumption for the PDF of the ABP modulus is acceptable, given the array geometry, the weight coefficients and the statistics of random errors. Where the Ricianity assumption is valid, the procedure to find an empirical equation for the probability that there are no overruns larger than a fixed size of a quantile BP function is shown. Unlike numerical assessments, the validity of these tools and procedures is not limited to the superdirective case, but is general. On the other hand, because of the peculiar importance of linear end-fire arrays [4], [6] in the field of superdirectivity, this paper confirms the Ricianity of their ABPs and opens the possibility of evaluating the robustness of a specific design by the quantile BP functions and the probability of no overruns larger than a fixed size. Furthermore, the quantile BP function (which depends on the parameters of the Rician PDF) can be adopted as the optimization target in new methods for designing robust superdirective arrays, for which the probability of exceeding a certain level is known.

This paper is organized as follows. Section II introduces the data model. Section III investigates the statistics of the ABP modulus, the possibility of adopting a Rician PDF and the related quantile functions. In Section IV the impact of different PDFs for random errors is analyzed and, then, used in Section V to numerically assess the validity of the Rician approximation and the relevance of the quantile functions. Section VI studies the correlation and independence between the BP lobes. Finally, Section VII explores the size of the overruns of a given quantile BP function, with the related probability. Some conclusions are drawn in Section VIII. Overall, the paper is organized into two parts: in the first (Sections II to V) Ricianity is studied and quantile functions are introduced; in the second (Sections VI and VII) the independence between side lobes is investigated and the probability of no overruns larger than a certain size is derived.

II. Data Model

In a spherical coordinate system [1], the components of the unit vector $\hat{\mathbf{u}}$ are related to the azimuth angle α and polar angle χ

[2]The WNG is the improvement in the signal-to-noise ratio obtained using the array and considering spatially uncorrelated noise; a kind of noise whose effect is similar to that of array errors.

as follows $\hat{\mathbf{u}} = \lfloor u_x, u_y, u_z \rfloor = [\sin\chi\cos\alpha, \sin\chi\sin\alpha, \cos\chi]$. Let us consider an arbitrary array of N elements whose l-th element, $l = 1, \ldots, N$, has a nominal position $\mathbf{p}_l^n = [x_l^n, y_l^n, z_l^n]$ and a nominal frequency response given by the complex function $A_l^n(f) = g_l^n(f)\exp[j\,\varphi_l^n(f)]$, where $g_l^n(f)$ is the nominal gain, $g_l^n(f) \geq 0$, and $\varphi_l^n(f)$ is the nominal phase. When random errors are introduced, the actual position of the l-th element becomes

$$\mathbf{p}_l = [x_l, y_l, z_l] = \mathbf{p}_l^n + \boldsymbol{\varepsilon}_l = \mathbf{p}_l^n + [\varepsilon_{x,l}, \varepsilon_{y,l}, \varepsilon_{z,l}] \quad (1)$$

where $\boldsymbol{\varepsilon}_l = [\varepsilon_{x,l}, \varepsilon_{y,l}, \varepsilon_{z,l}]$ is a vector of random variables (RVs) representing the position errors. The actual frequency response of the l-th element becomes

$$A_l(f) = g_l(f)\exp[j\varphi_l(f)] = A_l^n(f)\,\Sigma_l(f) \quad (2)$$

where

$$\begin{aligned}\Sigma_l(f) &= [1 + \delta_{g,l}(f)]\exp[j\,\delta_{\varphi,l}(f)] \\ &= \Lambda_l(f)\exp[j\,\delta_{\varphi,l}(f)]\end{aligned} \quad (3)$$

is a complex RV containing the gain error, $\delta_{g,l}(f)$, at frequency f, and the phase error, $\delta_{\varphi,l}(f)$, at the same frequency. On the one hand, the gain error is assumed such that $\Lambda_l(f) = [1 + \delta_{g,l}(f)] > 0$, assuring in this way that the actual gain $g_l(f)$ is not negative and greater than zero. On the other hand, it is reasonable to assume that $\Lambda_l(f) = [1 + \delta_{g,l}(f)] < K < \infty$, where K is a finite constant, arbitrarily high.

Let us consider a plane wave with wavefronts perpendicular to the unit vector $\hat{\mathbf{u}}$ impinging on the array, as sketched in Fig. 1(b). If $s_0(t)$ is the signal present at the origin of the coordinates, then the signal present at the generic position $\mathbf{p}$ is $s(t, \mathbf{p}) = s_0(t + \mathbf{p}\cdot\hat{\mathbf{u}}/c)$, where c is the wave propagation speed. Therefore, the l-th element of the array produces an electrical signal $q_l(t)$ whose spectrum is

$$Q_l(f) = A_l(f)\;S_0(f)\;\exp(jk\;\mathbf{p}_l\cdot\hat{\mathbf{u}}) \quad (4)$$

where k is the wavenumber, $k = 2\pi f/c$, and $S_0(f)$ is the Fourier transform of $s_0(t)$.

A far-field data-independent beamforming [1] that processes actual signals and is steered in the direction of the unit vector $\hat{\mathbf{u}}_0$ (which is defined by the steering angles α_0 and χ_0) produces an output beam signal $d(t)$ whose spectrum is

$$D(f) = \sum_{l=1}^{N} w_l(f)\,Q_l(f)\exp(-jk\;\mathbf{p}_l^n\cdot\hat{\mathbf{u}}_0) \quad (5)$$

where $w_l(f)$ is the complex-valued weight coefficient for the element l, at frequency f (see Fig. 1(b)). It can be written $w_l(f) = g_l^w(f)\exp\lfloor j\,\varphi_l^w(f)\rfloor$, where $g_l^w(f) \geq 0$. If the previous equations are inserted in (5), one obtains $D(f) = S_o(f)B(\hat{\mathbf{u}}, f)$, where

$$B(\hat{\mathbf{u}}, f) = \sum_{l=1}^{N} w_l(f)\,A_l^n(f)\,\Sigma_l(f)\exp\{jk\,[\mathbf{p}_l^n\cdot(\hat{\mathbf{u}} - \hat{\mathbf{u}}_0) + \boldsymbol{\varepsilon}_l\cdot\hat{\mathbf{u}}]\} \quad (6)$$

is the ABP, a complex function containing 5 RVs (i.e., $\varepsilon_{x,l}$, $\varepsilon_{y,l}$, $\varepsilon_{z,l}$, $\delta_{g,l}$, $\delta_{\varphi,l}$) for each array element. In view of subsequent developments, it is convenient to rewrite the ABP as

$$B(\hat{\mathbf{u}}, f) = \sum_{l=1}^{N} \Lambda_l^n(f)\,\Lambda_l(f)\exp\{j\,[\Phi_l^n(\hat{\mathbf{u}}, f) + \Phi_l(\hat{\mathbf{u}}, f)]\} \quad (7)$$

where

$$\Lambda_l^n(f) = g_l^n(f)\,g_l^w(f) \quad (8)$$

$$\Phi_l^n(\hat{\mathbf{u}}, f) = \varphi_l^n(f) + \varphi_l^w(f) + k\;\mathbf{p}_l^n\cdot(\hat{\mathbf{u}} - \hat{\mathbf{u}}_0) \quad (9)$$

$$\Phi_l(\hat{\mathbf{u}}, f) = \delta_{\varphi,l}(f) + k\;\boldsymbol{\varepsilon}_l\cdot\hat{\mathbf{u}} \quad (10)$$

If all the errors are zeroed, for each l, $\Phi_l(\hat{\mathbf{u}}, f) = 0$ and $\Lambda_l(f) = 1$. Thus, the NBP results to be

$$B^n(\hat{\mathbf{u}}, f) = \sum_{l=1}^{N} \Lambda_l^n(f)\exp[j\Phi_l^n(\hat{\mathbf{u}}, f)] \quad (11)$$

Because it was assumed that $\Lambda_l(f) \geq 0$, the real and imaginary parts of the ABP, can be expressed, respectively, as

$$\begin{aligned}B_R(\hat{\mathbf{u}}, f) &= \mathrm{Re}\{B(\hat{\mathbf{u}}, f)\} \\ &= \sum_{l=1}^{N} \Lambda_l^n(f)\,\Lambda_l(f)\cos[\Phi_l^n(\hat{\mathbf{u}}, f) + \Phi_l(\hat{\mathbf{u}}, f)]\end{aligned} \quad (12)$$

$$\begin{aligned}B_I(\hat{\mathbf{u}}, f) &= \mathrm{Im}\{B(\hat{\mathbf{u}}, f)\} \\ &= \sum_{l=1}^{N} \Lambda_l^n(f)\,\Lambda_l(f)\sin[\Phi_l^n(\hat{\mathbf{u}}, f) + \Phi_l(\hat{\mathbf{u}}, f)]\end{aligned} \quad (13)$$

III. Statistics of the ABP Modulus

To investigate the PDF of the ABP modulus three common assumptions on the random errors' PDFs are introduced [1], [3], [18]. To simplify the notation, when suitable, the dependence of the previous variables on f and $\hat{\mathbf{u}}$ will be omitted.

Assumption 1: The array elements have the same statistics. The PDFs $\beta_{\varepsilon_x}(\varepsilon_x)$, $\beta_{\varepsilon_y}(\varepsilon_y)$, $\beta_{\varepsilon_z}(\varepsilon_z)$, $\beta_{\delta_\varphi}(\delta_\varphi)$ and $\beta_{\delta_g}(\delta_g)$ are the functions that describe all the RVs $\varepsilon_{x,l}$, $\varepsilon_{y,l}$, $\varepsilon_{z,l}$, $\delta_{\varphi,l}$, $\delta_{g,l}$, $l = 1, \ldots, N$, respectively.

Assumption 2: Statistical independence. All the RVs $\varepsilon_{x,l}$, $\varepsilon_{y,l}$, $\varepsilon_{z,l}$, $\delta_{\varphi,l}$, $\delta_{g,l}$, $l = 1, \ldots, N$, are statistically independent; thus, all their joint PDFs are separable functions.[3]

Assumption 3: PDF symmetry. The PDFs $\beta_{\varepsilon_x}(\varepsilon_x)$, $\beta_{\varepsilon_y}(\varepsilon_y)$, $\beta_{\varepsilon_z}(\varepsilon_z)$ and $\beta_{\delta_\varphi}(\delta_\varphi)$ are even functions. This assumption is not applied to $\beta_{\delta_g}(\delta_g)$.

In addition, the errors $\varepsilon_{x,l}$, $\varepsilon_{y,l}$, $\varepsilon_{z,l}$, $\delta_{\varphi,l}$, $\delta_{g,l}$, $l = 1, \ldots, N$, are assumed to be RVs of continuous type.

The modulus of the ABP, $|B| = \sqrt{B_R^2 + B_I^2}$, has Rician PDF with distance parameter ν and scale parameter σ [35] if the three following conditions are satisfied:

[3]The statistical moments of the ABP modulus in the presence of correlated random errors, as well as the directivity reduction and steering direction fluctuation, have been investigated in [27], [28], [33].

(i) B_R is a Gaussian RV with mean value equal to $\nu\cos\xi$ and variance equal to σ^2;
(ii) B_I is a Gaussian RV with mean value equal to $\nu\sin\xi$ and variance equal to σ^2;
(iii) B_R and B_I are independent RVs;

where ξ is any real number. More specifically, the Rician PDF of a RV p is defined as

$$\beta_p(p) = \frac{p}{\sigma^2}\exp\left(\frac{-p^2-\nu^2}{2\sigma^2}\right) I_0\left(\frac{p\nu}{\sigma^2}\right) \tag{14}$$

where I_0 is the modified Bessel function of the first kind with order zero. The corresponding cumulative distribution function (CDF), $F_p(p)$, is defined as

$$F_p(p) = 1 - Q_1\left(\frac{\nu}{\sigma}, \frac{p}{\sigma}\right) \tag{15}$$

where Q_1 is the Marcum Q-function.

Equations (12) and (13) show that B_R and B_I are the sums of N terms, each of which is a function of the random errors that affect the l-th element. Since the errors affecting different array elements are independent RVs of continuous type, the N terms in the sums represent independent RVs of continuous type. The PDFs of such terms are not known and, in general, different from each other. Since the gain and phase dispersion is unavoidable for real transducers, for each term there exists a constant ϖ such that the term's variance is greater than ϖ. In addition, because it was assumed that $0 < \Lambda_l(f) < K$ and because $\Lambda_l^n(f)$ is also greater than zero and bounded from the above, all the PDFs of the N terms in (12) and (13) are equal to zero outside a finite interval $[0, A)$, A being a finite constant, no matter how large. According to [36], under these conditions the central limit theorem can be applied to independent not-identically distributed RVs. Therefore, the PDF of B_R and B_I is approximately Gaussian for a sufficiently great number of elements N. For the same reason, the PDF of every linear combination of B_R and B_I is also approximately Gaussian. Thus, B_R and B_I can be assumed to be jointly Gaussian RVs; the same conclusion already achieved in [5], [23], [25].

The requirements on the mean values of B_R and B_I (denoted by $\overline{B}_R$ and $\overline{B}_I$, respectively) are satisfied because $\overline{B}_R$ and $\overline{B}_I$ are the real and imaginary parts of the mean value, $\overline{B}$, of the ABP function given in (7). In particular, one can observe that $\nu = |\overline{B}|$.

To verify the remaining requirements settled by the conditions (i), (ii) and (iii), it is necessary to achieve compact equations for the mean powers of B_R and B_I, as well as for $\overline{B}_R$ and $\overline{B}_I$.

By indicating the expectation operator with $E\{.\}$, the mean power of B_R can be written

$$\overline{B_R^2} = E\left\{B_R^2\right\} = \Theta_1^R + \Theta_2^R \tag{16}$$

where

$$\Theta_1^R = E\left\{\sum_{l=1}^{N}(\Lambda_l^n)^2\Lambda_l^2\cos^2(\Phi_l^n + \Phi_l)\right\} \tag{17}$$

$$\Theta_2^R = E\left\{\sum_{l=1}^{N}\sum_{m=1,m\neq l}^{N}\Lambda_l^n\Lambda_m^n\Lambda_l\Lambda_m\cos(\Phi_l^n + \Phi_l) \cdot\cos(\Phi_m^n + \Phi_m)\right\} \tag{18}$$

Proposition 1: Under *Assumptions 1*, *2* and *3*, the terms Θ_1^R and Θ_2^R, used in (16) to compute the mean power of B_R, can be written as follows

$$\Theta_1^R = \frac{\overline{\Lambda}^2}{2}\sum_{l=1}^{N}(\Lambda_l^n)^2 + \frac{\overline{\Lambda}^2}{2}\mu_{2\Theta}\sum_{l=1}^{N}(\Lambda_l^n)^2\cos 2\Phi_l^n \tag{19}$$

$$\Theta_2^R = \overline{\Lambda}^2\mu_\Theta^2\sum_{l=1}^{N}\sum_{m=1,m\neq l}^{N}\Lambda_l^n\Lambda_m^n\cos\Phi_l^n\cos\Phi_m^n \tag{20}$$

where

$$\overline{\Lambda} = E\{\Lambda_l\} = 1 + \overline{\delta}_g, \quad \overline{\Lambda} > 0 \tag{21}$$

$$\overline{\Lambda}^2 = E\left\{\Lambda_l^2\right\} = 1 + 2\overline{\delta}_g + \overline{\delta_g^2} \tag{22}$$

$$\mu_\Theta = E\{\cos\Phi_l\} = E\{\cos(\delta_{\varphi,l})\}\,E\{\cos(k\,\boldsymbol{\varepsilon}_l\cdot\hat{\mathbf{u}})\} \tag{23}$$

$$\mu_{2\Theta} = E\{\cos(2\Phi_l)\} = E\{\cos(2\delta_{\varphi,l})\}\,E\{\cos(2k\,\boldsymbol{\varepsilon}_l\cdot\hat{\mathbf{u}})\} \tag{24}$$

$\overline{\delta}_g$ and $\overline{\delta_g^2}$ are the mean value and mean power, respectively, of the RV $\delta_{g,l}$, $l = 1, \ldots, N$. The *Proof* is provided in Appendix A.

If an analogous procedure is applied to study the mean power of B_I, the result is

$$\overline{B_I^2} = E\left\{B_I^2\right\} = \Theta_1^I + \Theta_2^I \tag{25}$$

where the terms Θ_1^I, Θ_2^I can be computed as follows

$$\Theta_1^I = \frac{\overline{\Lambda}^2}{2}\sum_{l=1}^{N}(\Lambda_l^n)^2 - \frac{\overline{\Lambda}^2}{2}\mu_{2\Theta}\sum_{l=1}^{N}(\Lambda_l^n)^2\cos 2\Phi_l^n \tag{26}$$

$$\Theta_2^I = \overline{\Lambda}^2\mu_\Theta^2\sum_{l=1}^{N}\sum_{m=1,m\neq l}^{N}\Lambda_l^n\Lambda_m^n\sin\Phi_l^n\sin\Phi_m^n \tag{27}$$

Moving from the mean powers to the mean values of B_R and B_I, the variables $\overline{\Lambda}$ and μ_Θ, and some of the results obtained above, can be used to easily achieve that

$$\overline{B}_R = \overline{\Lambda}\,\mu_\Theta\sum_{l=1}^{N}\Lambda_l^n\cos\Phi_l^n \tag{28}$$

$$\overline{B}_I = \overline{\Lambda}\,\mu_\Theta\sum_{l=1}^{N}\Lambda_l^n\sin\Phi_l^n \tag{29}$$

From these equations, the squares of mean values result to be

$$\overline{B}_R^2 = \overline{\Lambda}^2\,\mu_\Theta^2\sum_{l=1}^{N}\sum_{m=1}^{N}\Lambda_l^n\Lambda_m^n\cos\Phi_l^n\cos\Phi_m^n$$

$$= \Theta_2^R + \overline{\Lambda}^2\,\mu_\Theta^2\sum_{l=1}^{N}(\Lambda_l^n)^2\cos^2\Phi_l^n \tag{30}$$

$$\overline{B}_I^2 = \overline{\Lambda}^2\,\mu_\Theta^2 \sum_{l=1}^{N}\sum_{m=1}^{N} \Lambda_l^n \Lambda_m^n\,\sin\Phi_l^n\,\sin\Phi_m^n$$

$$= \Theta_2^I + \overline{\Lambda}^2\,\mu_\Theta^2 \sum_{l=1}^{N} (\Lambda_l^n)^2\,\sin^2\Phi_l^n \tag{31}$$

The previous results allow one to conclude that the variances of the real and imaginary parts of the ABP, σ_R^2 and σ_I^2, can be written as

$$\sigma_R^2 = \overline{B_R^2} - \overline{B}_R^2 = \frac{\overline{\Lambda}^2}{2}\sum_{l=1}^{N}(\Lambda_l^n)^2 + \frac{\overline{\Lambda}^2}{2}\mu_{2\Theta}\sum_{l=1}^{N}(\Lambda_l^n)^2\cos 2\Phi_l^n$$

$$-\,\overline{\Lambda}^2\,\mu_\Theta^2 \sum_{l=1}^{N} (\Lambda_l^n)^2\,\cos^2\Phi_l^n \tag{32}$$

$$\sigma_I^2 = \overline{B_I^2} - \overline{B}_I^2 = \frac{\overline{\Lambda}^2}{2}\sum_{l=1}^{N}(\Lambda_l^n)^2 - \frac{\overline{\Lambda}^2}{2}\,\mu_{2\Theta}\sum_{l=1}^{N}(\Lambda_l^n)^2\cos 2\Phi_l^n$$

$$-\,\overline{\Lambda}^2\,\mu_\Theta^2 \sum_{l=1}^{N} (\Lambda_l^n)^2\,\sin^2\Phi_l^n \tag{33}$$

and turn out to be different from each other. Even if this difference prevents conditions (i) and (ii) from being fully satisfied, if the difference between the two variances is small the Rician function could still be a good approximation for the PDF of the ABP module. To investigate this point, the normalized difference Δ,

$$\Delta = \frac{\sigma_R^2 - \sigma_I^2}{\sigma_R^2 + \sigma_I^2} \tag{34}$$

ranging between -1 and 1, will be adopted. To help the computation of Δ, after some mathematics, the difference and sum between the variances can be compacted as follows

$$\sigma_R^2 - \sigma_I^2 = \left(\overline{\Lambda}^2\mu_{2\Theta} - \overline{\Lambda}^2\mu_\Theta^2\right)\sum_{l=1}^{N}(\Lambda_l^n)^2\cos 2\Phi_l^n \tag{35}$$

$$\sigma_R^2 + \sigma_I^2 = \left(\overline{\Lambda}^2 - \overline{\Lambda}^2\mu_\Theta^2\right)\sum_{l=1}^{N}(\Lambda_l^n)^2 \tag{36}$$

Assuming B_R and B_I to be jointly Gaussian RVs, the condition (iii) is verified if they are uncorrelated, i.e., if their covariance, $\eta_{R,I}$, is equal to zero.

Proposition 2: Under *Assumptions 1*, *2* and *3*, the expectation $E\{B_R B_I\}$ can be written as $E\{B_R B_I\} = \Theta_1^\eta + \Theta_2^\eta$, where

$$\Theta_1^\eta = \frac{\overline{\Lambda}^2}{2}\mu_{2\Theta}\sum_{l=1}^{N}(\Lambda_l^n)^2\sin 2\Phi_l^n \tag{37}$$

$$\Theta_2^\eta = \overline{\Lambda}^2\mu_\Theta^2\sum_{l=1}^{N}\sum_{m=1,m\neq l}^{N}\Lambda_l^n\Lambda_m^n\cos\Phi_l^n\,\sin\Phi_m^n \tag{38}$$

and the covariance, defined as $\eta_{R,I} = E\{B_R B_I\} - \overline{B}_R\overline{B}_I$, results to be

$$\eta_{R,I} = \left(\overline{\Lambda}^2\mu_{2\Theta} - \overline{\Lambda}^2\mu_\Theta^2\right)\frac{1}{2}\sum_{l=1}^{N}(\Lambda_l^n)^2\sin 2\Phi_l^n \tag{39}$$

The *Proof* is provided in Appendix B. Therefore, in general, the covariance is not zero and the condition (iii) is not fully satisfied. However, as for conditions (i) and (ii), the covariance could have a very small value and not prevent the Rician function from being a good approximation. To investigate the point, the correlation coefficient ρ,

$$\rho = \frac{\eta_{R,I}}{\sigma_R\sigma_I} \tag{40}$$

ranging between -1 and 1, will be adopted.

A. ABP Mean Value and ABP Mean Power

Up to this point, attention has been focused on the PDF of the ABP modulus. The study performed can also be applied to calculate some moments of the ABP, remembering that B is a complex-valued function. In particular, using the equations obtained for B^n, $\overline{B}_R$ and $\overline{B}_I$, the relations among the ABP mean value, its modulus and the NBP can be derived

$$\overline{B} = E\{B\} = \overline{B}_R + j\overline{B}_I = \overline{\Lambda}\,\mu_\Theta B^n \tag{41}$$

$$\left|\overline{B}\right| = \overline{\Lambda}\,|\mu_\Theta B^n| \tag{42}$$

The ABP mean power can also be computed, yielding

$$\overline{|B|^2} = E\left\{|B|^2\right\} = \overline{B_R^2} + \overline{B_I^2} = \Theta_1^R + \Theta_2^R + \Theta_1^I + \Theta_2^I \tag{43}$$

Because B is a complex-valued function, its mean power corresponds to the power of its modulus. Clearly, this is not true for the mean value. Thus, it is important to distinguish between the modulus of the ABP mean value [introduced in (42)] and the mean value of the ABP modulus that will be introduced in Section III.C. After some mathematics, the mean power can be compacted in the following way

$$\overline{|B|^2} = \left(\overline{\Lambda}^2 - \overline{\Lambda}^2\,\mu_\Theta^2\right)\sum_{l=1}^{N}(\Lambda_l^n)^2 + \left|\overline{B}\right|^2 \tag{44}$$

where the first addend of the right-hand side represents the variance of the ABP, σ_B^2.

B. Rician PDF Parameters

Assuming the terms Δ and ρ are both close to zero and the array has a sufficient number of elements to apply the central limit theorem, the Rician PDF can be considered a good approximation for the statistics of the modulus of the ABP. Based on the previous results, the parameters ν and σ of such a PDF can be calculated as follows

$$\nu = \left|\overline{B}\right| = \overline{\Lambda}\,|\mu_\Theta B^n| \tag{45}$$

$$\sigma^2 = \frac{\sigma_R^2 + \sigma_I^2}{2} = \left(\overline{\Lambda}^2 - \overline{\Lambda}^2\mu_\Theta^2\right)\frac{1}{2}\sum_{l=1}^{N}(\Lambda_l^n)^2 \tag{46}$$

The average between σ_R^2 and σ_I^2 is used to find the value for σ^2, because the two terms are not equal and their difference was assumed to be minor. Both ν and σ depend on $\hat{\mathbf{u}}$ because μ_Θ and B^n depend on it. Obviously, they also depend on the frequency f.

C. Mean Value and Quantile Functions of the ABP Modulus

Assuming the modulus of the ABP can be approximated, at a given direction $\hat{\mathbf{u}}$, through a RV with Rician statistics, its mean value

$$B_m(\hat{\mathbf{u}}) = \overline{|B(\hat{\mathbf{u}})|} = E\{|B(\hat{\mathbf{u}})|\} \tag{47}$$

can be computed by the moment equation given in [35]. This function is obviously different from the modulus of the mean ABP, $|\overline{B(\hat{\mathbf{u}})}|$, defined in (42), which is a scaled version of the NBP modulus.

In addition, the Rician CDF in (15) for the RV $|B(\hat{\mathbf{u}})|$ allows one to introduce the quantile function of the ABP modulus, $B_{q,\gamma}(\hat{\mathbf{u}})$,

$$B_{q,\gamma}(\hat{\mathbf{u}}) = F^{-1}_{|B(\hat{\mathbf{u}})|}(\gamma) \tag{48}$$

where $F^{-1}_{|B(\hat{\mathbf{u}})|}(\cdot)$ represents the inverse of the CDF and $\gamma \in [0, 1]$. For each $\hat{\mathbf{u}}$, the equation provides the value $B_{q,\gamma}$ for which the probability that the modulus of the ABP is less than or equal to $B_{q,\gamma}$ is equal to γ. The clear mathematical meaning of quantile functions allows for potential adoption of them as targets in a superdirective array optimization process, where the impact of errors is considered through their PDFs.

IV. PDFs for Random Errors

The variables μ_Θ and $\mu_{2\Theta}$, contained in the equations to compute $\nu, \sigma, \Delta, \rho$ and the ABP mean power, depend on the statistics of the phase and position errors. In this section the computation of μ_Θ and $\mu_{2\Theta}$ is addressed when phase and position errors can be described by uniform or Gaussian PDFs. In addition, a general formulation for the case in which the position errors present a spherical symmetry is provided. Before introducing specific PDFs, it is important to highlight that, applying error independence and even symmetry, (23) and (24) can be expanded as follows

$$\begin{aligned}\mu_\Theta &= E\{\cos\Phi_l\} = E\{\cos(\delta_{\varphi,l})\}\, E\{\cos(k\ \varepsilon_{x,l}\ u_x)\} \\ &\quad \cdot E\{\cos(k\ \varepsilon_{y,l}\ u_y)\}\, E\{\cos(k\ \varepsilon_{z,l}\ u_z)\}\end{aligned} \tag{49}$$

$$\begin{aligned}\mu_{2\Theta} &= E\{\cos(2\Phi_l)\} = E\{\cos(2\delta_{\varphi,l})\}\, E\{\cos(2k\ \varepsilon_{x,l}\ u_x)\} \\ &\quad \cdot E\{\cos(2k\ \varepsilon_{y,l}\ u_y)\}\, E\{\cos(2k\ \varepsilon_{z,l}\ u_z)\}\end{aligned} \tag{50}$$

Gaussian PDFs. Starting from the following relation [37]

$$\int_{-\infty}^{\infty} \cos(bx)\, \frac{1}{\sqrt{2\pi\sigma_x^2}} \exp\left(\frac{-x^2}{2\sigma_x^2}\right) dx = \exp\left(-\frac{b^2\sigma_x^2}{2}\right) \tag{51}$$

and assuming $\beta_{\varepsilon_x}(\varepsilon_x)$, $\beta_{\varepsilon_y}(\varepsilon_y)$, $\beta_{\varepsilon_z}(\varepsilon_z)$ and $\beta_{\delta_\varphi}(\delta_\varphi)$ to be Gaussian PDFs with zero mean and variance $\sigma^2_{\varepsilon_x}, \sigma^2_{\varepsilon_y}, \sigma^2_{\varepsilon_z}, \sigma^2_{\delta_\varphi}$, respectively, the variables μ_Θ and $\mu_{2\Theta}$ result to be

$$\mu_\Theta = \exp\left(-\frac{\sigma^2_{\delta_\varphi} + k^2u_x^2\sigma^2_{\varepsilon_x} + k^2u_y^2\sigma^2_{\varepsilon_y} + k^2u_z^2\sigma^2_{\varepsilon_z}}{2}\right) \tag{52}$$

$$\mu_{2\Theta} = \exp\left[-2\left(\sigma^2_{\delta_\varphi} + k^2u_x^2\sigma^2_{\varepsilon_x} + k^2u_y^2\sigma^2_{\varepsilon_y} + k^2u_z^2\sigma^2_{\varepsilon_z}\right)\right] \tag{53}$$

If the position errors along the three axes have the same variance σ^2_ε, one can compact as

$$\mu_\Theta = \exp\left(-\frac{\sigma^2_{\delta_\varphi}}{2}\right)\exp\left(-\frac{k^2\sigma^2_\varepsilon}{2}\right) \tag{54}$$

$$\mu_{2\Theta} = \exp\left(-2\sigma^2_{\delta_\varphi}\right)\exp\left(-2k^2\sigma^2_\varepsilon\right) \tag{55}$$

It is interesting to note that in this case the terms μ_Θ and $\mu_{2\Theta}$ (and, in turn, scale parameter σ of the Rician PDF) do not depend on the arrival direction $\hat{\mathbf{u}}$. Moreover, the impact of position errors grows with frequency because the ratio between the variance and the wavelength increases.

Uniform PDFs. Starting from the relation

$$\int_{-\Delta}^{\Delta} \cos(bx)\, \frac{1}{2\Delta} dx = \operatorname{sinc}\left(\frac{\Delta b}{\pi}\right) \tag{56}$$

where $\operatorname{sinc}(a) = \sin(\pi a)/\pi a$, and assuming $\beta_{\varepsilon_x}(\varepsilon_x)$, $\beta_{\varepsilon_y}(\varepsilon_y)$, $\beta_{\varepsilon_z}(\varepsilon_z)$ and $\beta_{\delta_\phi}(\delta_\varphi)$ to be uniform PDFs on the intervals $[-\Delta_x, \Delta_x]$, $[-\Delta_y, \Delta_y]$, $[-\Delta_z, \Delta_z]$ and $[-\Delta_\varphi, \Delta_\varphi]$, respectively, the variables μ_Θ and $\mu_{2\Theta}$ result to be

$$\begin{aligned}\mu_\Theta &= \operatorname{sinc}\left(\frac{\Delta_\varphi}{\pi}\right)\operatorname{sinc}\left(\frac{ku_x\Delta_x}{\pi}\right) \\ &\quad \operatorname{sinc}\left(\frac{ku_y\Delta_y}{\pi}\right)\operatorname{sinc}\left(\frac{ku_z\Delta_z}{\pi}\right)\end{aligned} \tag{57}$$

$$\begin{aligned}\mu_{2\Theta} &= \operatorname{sinc}\left(\frac{2\Delta_\varphi}{\pi}\right)\operatorname{sinc}\left(\frac{2ku_x\Delta_x}{\pi}\right) \\ &\quad \operatorname{sinc}\left(\frac{2ku_y\Delta_y}{\pi}\right)\operatorname{sinc}\left(\frac{2ku_z\Delta_z}{\pi}\right)\end{aligned} \tag{58}$$

Spherical symmetry of the position errors. Although the term $k\boldsymbol{\varepsilon}_l \cdot \hat{\mathbf{u}}$ contained in (23) and (24) causes μ_Θ and $\mu_{2\Theta}$ to be dependent on the direction $\hat{\mathbf{u}}$, it has been shown that when $\varepsilon_{x,l}$, $\varepsilon_{y,l}$ and $\varepsilon_{z,l}$ have uncorrelated zero-mean Gaussian PDFs with the same variance, the dependence on $\hat{\mathbf{u}}$ is avoided. More in general, the dependence on $\hat{\mathbf{u}}$ is avoided for any spherically symmetric PDF of the position errors $\boldsymbol{\varepsilon}_l$. According to [3], assuming the statistics of the position errors $\boldsymbol{\varepsilon}_l$ has a spherical symmetry and is the same for all the array elements, Appendix C demonstrates that

$$E\{\cos(k\boldsymbol{\varepsilon}_l \cdot \hat{\mathbf{u}})\} = \int_0^\infty \operatorname{sinc}\left(\frac{kr}{\pi}\right)\beta_r(r)\, dr \tag{59}$$

$$E\{\cos(2k\boldsymbol{\varepsilon}_l \cdot \hat{\mathbf{u}})\} = \int_0^\infty \operatorname{sinc}\left(\frac{2kr}{\pi}\right)\beta_r(r)\, dr \tag{60}$$

where r is modulus of the error vector $\boldsymbol{\varepsilon}_l$ and $\beta_r(r)$ is the PDF of such a RV. As anticipated above, the two integrals do not depend on $\hat{\mathbf{u}}$. If the variables $\varepsilon_{x,l}$, $\varepsilon_{y,l}$ and $\varepsilon_{z,l}$ have zero-mean Gaussian PDFs with variance σ^2_ε, $\beta_r(r)$ results to be a Maxwell-Boltzmann PDF with a scale parameter σ_ε and the integrals in (59) and (60) result to be $\exp(-k^2\sigma^2_\varepsilon/2)$ and $\exp(-2k^2\sigma^2_\varepsilon)$, respectively, in accordance with (54) and (55).

V. Numerical Assessment: Rician Approximation and Quantile Functions

Although the three conditions necessary to demonstrate that the ABP modulus follows the Rician statistics are not completely satisfied, the possibility that the deviations from these necessary conditions are small and that the Rician PDF represents a good approximation should be contemplated. In this section, the normalized difference between the two variances, Δ, and the correlation coefficient, ρ, are numerically analyzed with reference to some cases of practical interest. In addition, the quantile functions for these cases are analyzed, compared with the mean power of the ABP modulus and used to evaluate different options for designing a superdirective array.

A. Numerical Setup

A linear array of equally spaced elements placed on the z-axis is considered. The elements are assumed to be point-like and omnidirectional, placed at the nominal positions $\mathbf{p}_l^n = [0, 0, dl - d(N+1)/2]$, $l = 1, \ldots, N$, where d is the inter-element spacing. Without any loss of generality their nominal gains g_l^n are set equal to one and their nominal phases φ_l^n are set equal to zero. Given that for a linear array placed on the z-axis the polar angle χ represents the grazing angle, as visible in Fig. 1(b), the broadside angle θ can be defined as

$$\theta = \frac{\pi}{2} - \chi, \tag{61}$$

and the NBP depends only on θ, irrespective of α. Because the focus here is primarily on the statistics of superdirective BPs, the steering direction is set at end-fire (i.e., $\theta_0 = 90°$) where the maximum amount of superdirectivity is obtained [4], [6], [7]. An example of superdirective end-fire BP is shown in Fig. 1(a).

Concerning the complex weight coefficients w_l used for the beamforming operation, for a given combination between N and d/λ (λ being the wavelength, $\lambda = c/f$), they are computed through the maximization of the directivity subject to a constraint on the minimum value of the WNG. This constrained optimization is a classical approach to achieve robust superdirective performance, as described in [1], [4], [19]. More in detail, the directivity and WNG can be written in matrix form by defining a column vector $\mathbf{w}$ for which the l-th element is $\mathbf{w}[l] = w_l$, $l = 1, 2, \ldots, N$, and a square matrix $\mathbf{Q}$ for which the element in the l-th row and m-th column is:

$$\mathbf{Q}[l, m] = \exp[jk(z_l^n - z_m^n)]\,\mathrm{sinc}[k(z_m^n - z_l^n)/\pi] \tag{62}$$

Using this notation, the directivity, D, and WNG, G, can be defined [1], [22] as follows

$$D = |B^n(\theta_0)|^2 \left(\frac{1}{2}\int_0^\pi |B^n(\theta)|^2 \sin\theta d\theta\right)^{-1} = \frac{\mathbf{w}^H\mathbf{J}\mathbf{w}}{\mathbf{w}^H\mathbf{Q}\mathbf{w}} \tag{63}$$

$$G = |B^n(\theta_0)|^2 \left(\sum_{l=1}^N |w_l|^2\right)^{-1} = \frac{\mathbf{w}^H\mathbf{J}\mathbf{w}}{\mathbf{w}^H\mathbf{w}} \tag{64}$$

where ^{H} indicates the complex-conjugate transpose and $\mathbf{J}$ is a square matrix of ones of size N. Following a common practice, the lower bound for the WNG is set equal to 0 dB and the optimization is performed by solving a quadratically constrained quadratic program by a convex optimization tool [22]. The WNG constraint is not only used for data-independent beamforming; it has also been used to improve the robustness of data-dependent beamforming techniques [38], e.g., the norm-constrained Capon beamforming [39], also referred to as minimum variance distortionless response beamforming with WNG constraint [40]. In these techniques, the matrix $\mathbf{Q}$ is replaced by the covariance matrix of the array signals. The data-dependent solution is equivalent to the data-independent one if an isotropic noise field is assumed to be the only signal that impinges on the array.

TABLE I
Number of Elements, N, Inter-Element Spacing, d/λ, and Error PDF Set (See Table II) for the Linear Array Combinations From C-1 to C-8

Combin.	N	d/λ	PDF set
C-1	8	0.05	S_1
C-2	8	0.05	S_2
C-3	8	0.3	S_1
C-4	8	0.3	S_2
C-5	16	0.05	S_1
C-6	16	0.05	S_2
C-7	16	0.3	S_1
C-8	16	0.3	S_2

TABLE II
Zero-Mean PDFs and Standard Deviations for the Array Random Errors Assumed in Sets S_1 and S_2. The Same PDF Is Assumed for the Position Errors ε_x, ε_y, ε_z

PDF set	Gain error δ_g Zero-mean uniform PDF	Phase error δ_φ Zero-mean Gaussian PDF	Position errors ε_x, ε_y, ε_z Zero-mean Gaussian PDF
S_1	$\sigma_{\delta_g} = 0.1 \Leftrightarrow \delta_g \in [-0.17, 0.17]$	$\sigma_{\delta_\varphi} = 0.1$ rad	$\sigma_\varepsilon = 0.005\lambda$
S_2	$\sigma_{\delta_g} = 0.2 \Leftrightarrow \delta_g \in [-0.35, 0.35]$	$\sigma_{\delta_\varphi} = 0.2$ rad	$\sigma_\varepsilon = 0.01\lambda$

Eight combinations among N, d/λ, and the random errors' statistics are considered. Table I contains the values related to each combination (from C-1 to C-8) and Table II describes the characteristics of the two sets of PDFs, S_1 and S_2, that are adopted to model the random errors. In particular, the standard deviation for the position errors σ_ε is expressed in terms of the wavelength λ. This means that the accuracy of the element placement increases when the wavelength decreases. In other words, if the frequency increases, the inter-element spacing decreases (because d/λ is set to be constant) and a better geometrical precision in the elements' placement is expected. Table III reports the nominal directivity [1] achieved by the robust superdirective beamforming (optimum weight coefficients) in comparison with the directivity achieved using uniform weight coefficients. For the four combinations of N and d/λ considered, the directivity increase provided by optimum weights is between 5.1 and 6.4 dB.

TABLE III
DIRECTIVITY OF THE END-FIRE NBP OBTAINED WITH UNIFORM WEIGHTS AND OPTIMUM WEIGHTS (MAX. DIRECTIVITY WITH A 0 dB WNG LOWER BOUND). FOUR COMBINATIONS OF N AND d/λ ARE CONSIDERED

Combination	Directivity, uniform w_I	Directivity, optimum w_I
C-1, C-2	2.5 dB	8.6 dB
C-3, C-4	9.7 dB	14.8 dB
C-5, C-6	5.3 dB	11.7 dB
C-7, C-8	12.8 dB	18.6 dB

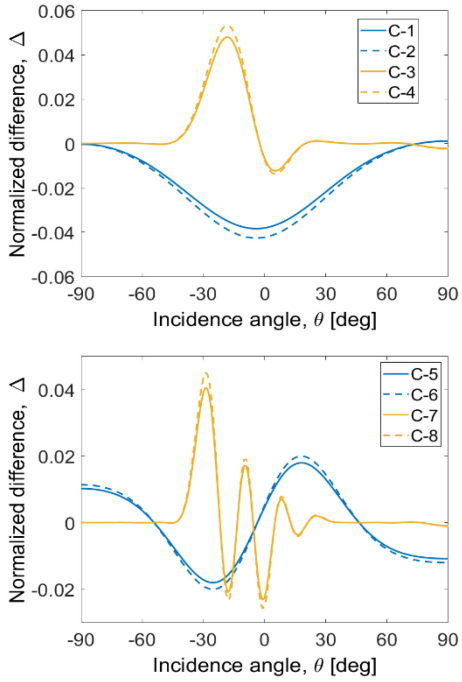

Fig. 2. Normalized difference, Δ, between the variances of the real and imaginary parts of the ABP, for (up) 8-element and (down) 16-element end-fire linear arrays.

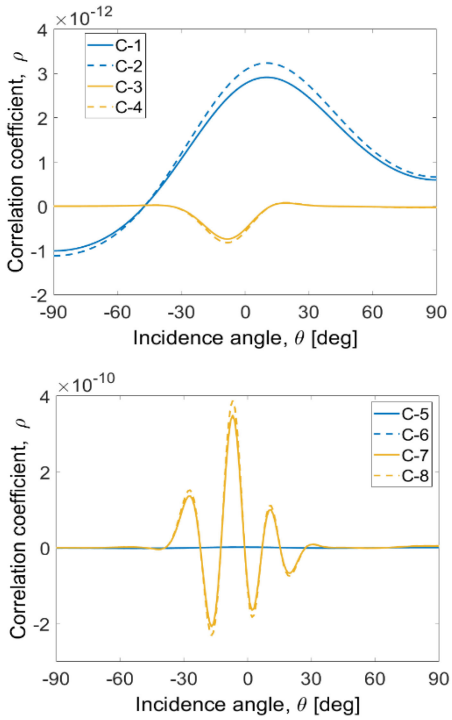

Fig. 3. Correlation coefficient, ρ, between the real and imaginary parts of the ABP, for (up) 8-element and (down) 16-element end-fire linear arrays.

B. Validity of the Rician Approximation

The normalized difference between the two variances, Δ, is displayed in Fig. 2 as a function of the incidence angle θ (irrespective of α). The increase of the error magnitude (i.e., moving from S_1 to S_2) and the increase of the ratio d/λ (i.e., moving from 0.05 to 0.3) weakly raise the maximum of the Δ absolute value. In any case, for the eight combinations considered, the maximum of the Δ absolute value does not exceed 0.053 (for C-4 and $\theta = -18°$). The correlation coefficient between the ABP real and imaginary parts, ρ, is displayed in Fig. 3. For the eight combinations considered the ρ absolute value does not exceed $4{\cdot}10^{-10}$. Recalling that the real and imaginary parts of the ABP tend to be Gaussian as N increase, the very small values assumed by their correlation coefficient allow one to consider B_R and B_I as independent RVs, supporting the adoption of the Rician statistics for the ABP modulus. Overall, the main obstacle to the adoption of the Rician statistics is the difference between the variances of B_R and B_I. Although such a difference is limited, it cannot be considered fully negligible.

To verify that, despite the deviations from the conditions (i)-(iii), the Rician PDF is a suitable approximation for the statistics of the ABP modulus, attention is focused on the combination C-4. Fig. 1(a) shows the NBP modulus obtained with superdirective weights in comparison with that obtained with uniform weights. Both superdirective and uniform weights are normalized in such a way that the maximum of the NBP modulus is one. Assuming the PDF set S_2 for the statistics of errors, the scale parameter σ for the Rician PDF is 0.204 (independent of θ) and the distance parameter ν is equal to the NBP modulus [see (45)] scaled by the factor $\overline{\Lambda}|\mu_\Theta|$. The latter is 0.978, independent of θ. Based on these data, a Rician PDF for each point of the ABP modulus can be established. Fig. 1(a) shows also the mean value of the Rician RV as a function of the incidence angle, expressed in logarithmic scale, avoiding any additional normalization. Fig. 4 shows the Rician PDFs computed for the combination C-4 at three incidence angles: $\theta = -18°$, $\theta = 65°$ and $\theta = 90°$. According to Fig. 1(a), these angles represent three different conditions for the statistics of the ABP modulus, i.e., low, intermediate and high nominal levels, respectively. Moreover, the condition C-4 and $\theta = -18°$ identifies the maximum of the Δ absolute value, as shown in Fig. 2. The Rician PDF moves from a profile close to the Rayleigh PDF ($\theta = -18°$) to a profile close to the Gaussian PDF ($\theta = 90°$). These PDFs are compared with the histograms computed from 10^6 independent realizations of the ABP for the combination C-4, using 100 quantization intervals uniformly spanning the interval [0, 2]. The relative frequency of each interval is divided by the quantization step, obtaining in this way histograms with total area equal to one. Very good matching can be observed between the PDFs and the related histograms.

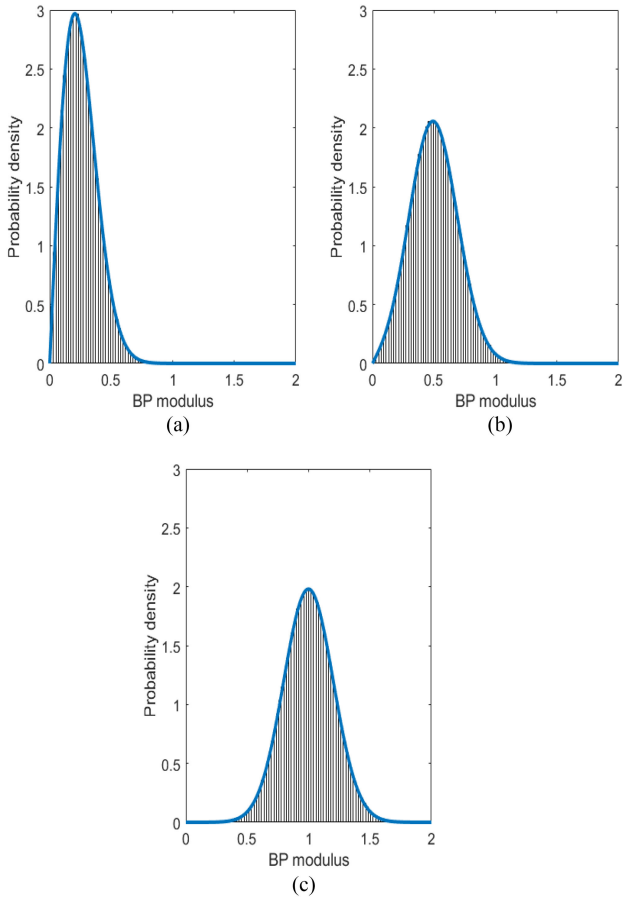

Fig. 4. Rician PDFs for the ABP modulus (in linear scale, blue line) of the C-4 array, compared with the normalized histograms of 10^6 independent realizations. (a) $\theta = -18°$; (b) $\theta = 65°$; (c) $\theta = 90°$.

A further and more general assessment is performed through the Kolmogoroff-Smirnov (KS) hypothesis test [36]. For each combination, from C-1 to C-8, a number G of independent realizations of the ABP, at a given incidence angle θ, are computed. The H_0 hypothesis is that the sample of size G is from a Rician CDF whose parameters ν and σ are given by (45) and (46). This hypothesis is rejected if the KS statistic, q, is larger than the critical value, q_{cv}, which is a function of the significance level (set equal to 0.05) and the sample size G [36]. Specifically, the sample size G is set equal to 10^3, the generation of the sample is repeated 10^2 times and the KS test is carried out for each sample. In addition, this procedure is performed for θ ranging from $-90°$ to $90°$, with steps of $5°$. Fig. 5 shows the average of q, compared with the critical value q_{cv}. Fig. 6 shows the relative frequency for which the H_0 hypothesis is not rejected by the KS test. One can observe that the average of the test statistic q always stays well below its critical value and the non-rejection percentage for the H_0 hypothesis is always greater than 94%. The latter outcome is coherent with the significance level equal to 0.05, which expresses the probability of rejecting the H_0 hypothesis when the sample is really taken from a Rician CDF. Therefore, for the eight array combinations examined, the Rician density represents a good approximation of their ABP modulus PDF.

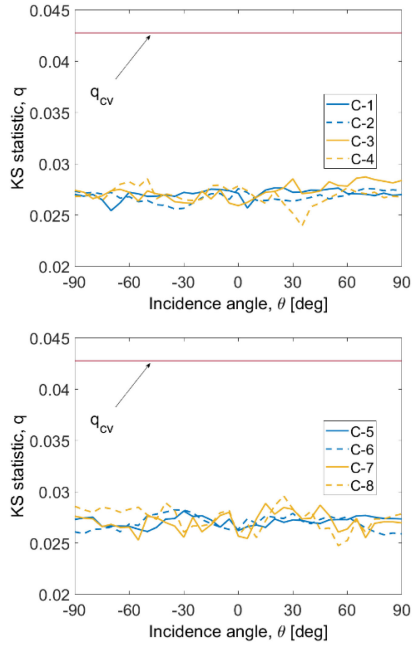

Fig. 5. KS test for the hypothesis that 10^3 random realizations of the ABP are from the Rician PDF. The average of the KS statistic after 100 test repetitions, as a function of the incidence angle, is compared with the critical value, for (up) 8-element and (down) 16-element end-fire linear arrays.

C. ABP Mean Power and Quantile Functions

To investigate the meaning of the ABP mean power (also called EBPP, often adopted to assess the array robustness in the literature), the function $\overline{|B(\hat{\mathbf{u}})|^2}$ can be compared in dB-scale with the mean value of the ABP modulus, $|\overline{B(\hat{\mathbf{u}})}|$, and the median value of the ABP modulus, i.e., the function $B_{q,0.50}(\hat{\mathbf{u}})$. An example for the combinations C-2 and C-4 is shown in Fig. 7, where $20\log[|B^n(\hat{\mathbf{u}})|]$, $10\log[\overline{|B(\hat{\mathbf{u}})|^2}]$, $20\log[|\overline{B(\hat{\mathbf{u}})}|]$ and $20\log[B_{q,0.50}(\hat{\mathbf{u}})]$ are compared, avoiding any normalization. The modulus of the mean ABP, $|\overline{B(\hat{\mathbf{u}})}|$, is not considered because it is almost overlapped on the modulus of the NBP, $|B^n(\hat{\mathbf{u}})|$, as already observed. In both panels of Fig. 7, the mean value and median value of the ABP modulus are very close each other: the maximum distance is in the side-lobe region and does not exceed 0.6 dB. In the main lobe region, where the Rician PDF tends to become a Gaussian function (see Fig. 4(c)), the median and mean values are almost equal. In dB scale, the ABP mean power is slightly higher than the mean of the ABP modulus: in the side-lobe region the two curves have an almost constant distance of approximately 1 dB. It has been verified that these observations also hold for the combinations other than C-2 and C-4. Thus, the ABP mean power profile is very similar to that of the mean value of the ABP modulus, although in the side-lobe region a small difference is observed.

Figs. 8 and 9 show the quantile functions $B_{q,0.90}(\hat{\mathbf{u}})$ and $B_{q,0.99}(\hat{\mathbf{u}})$ for the arrays with 8 and 16 elements, respectively, in comparison with the NBP and the mean value of the ABP modulus. These quantile functions are significantly higher than the NBP (including the main-lobe region) and, obviously, their level increases moving from the error set S_1 to the error set S_2.

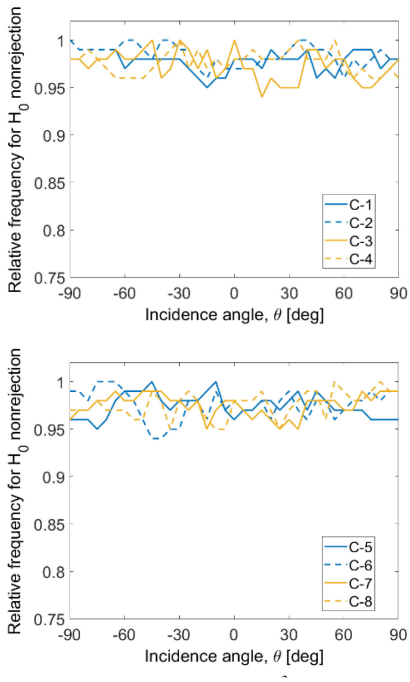

Fig. 6. KS test for the hypothesis that 10^3 random realizations of the ABP are from the Rician PDF. Relative frequency of non-rejection after 100 test repetitions, as a function of the incidence angle, for (up) 8-element and (down) 16-element end-fire linear arrays.

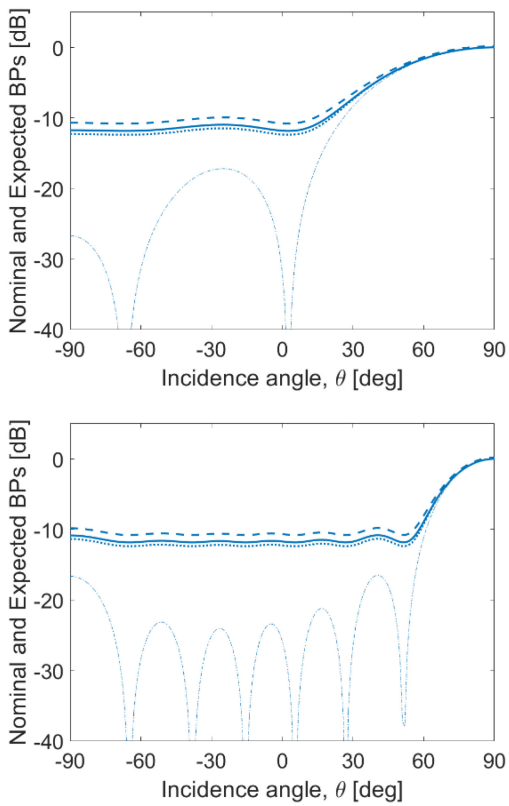

Fig. 7. Comparison in dB-scale of: NBP (dash-dotted); mean of the ABP modulus (solid); median of the ABP modulus (dotted); ABP mean power (dashed). (up) C-2; (down) C-4.

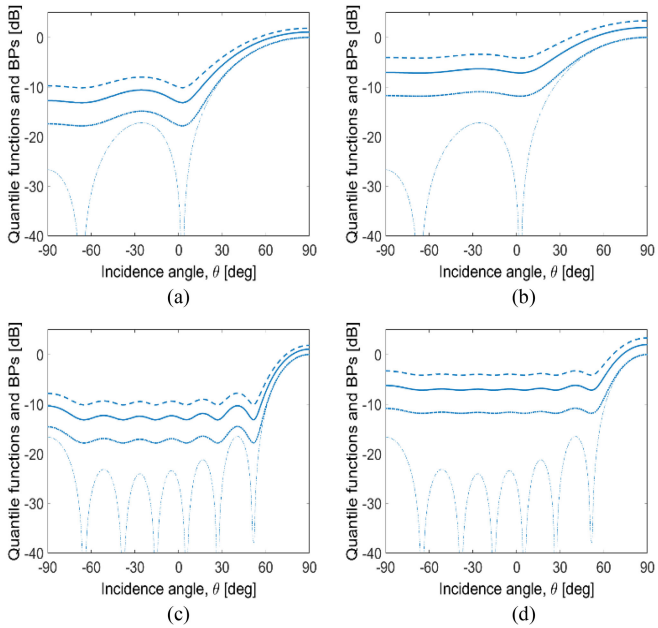

Fig. 8. NBP (dash-dotted). Mean of the ABP modulus (dotted). Quantile function $\gamma = 0.90$ (solid). Quantile function $\gamma = 0.99$ (dashed). (a) C-1; (b) C-2; (c) C-3; (d) C-4.

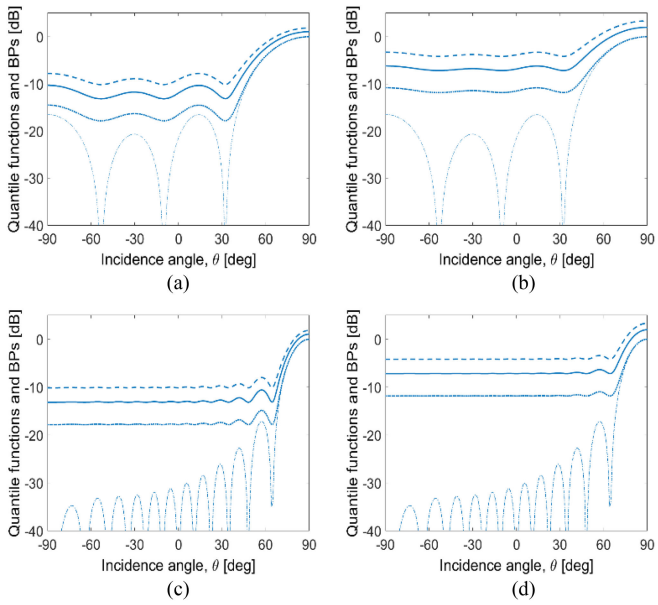

Fig. 9. NBP (dash-dotted). Mean of the ABP modulus (dotted). Quantile function $\gamma = 0.90$ (solid). Quantile function $\gamma = 0.99$ (dashed). (a) C-5; (b) C-6; (c) C-7; (d) C-8.

D. Superdirective Array Design Through Quantile Functions: An Example

This subsection evaluates two superdirective weighting windows for the C-3 end-fire array, obtained from the constrained optimization procedure described in Section V.A. Specifically, the directivity is maximized with the lower bound for the WNG set at two different values: -5 dB and 5 dB. The NBPs achieved

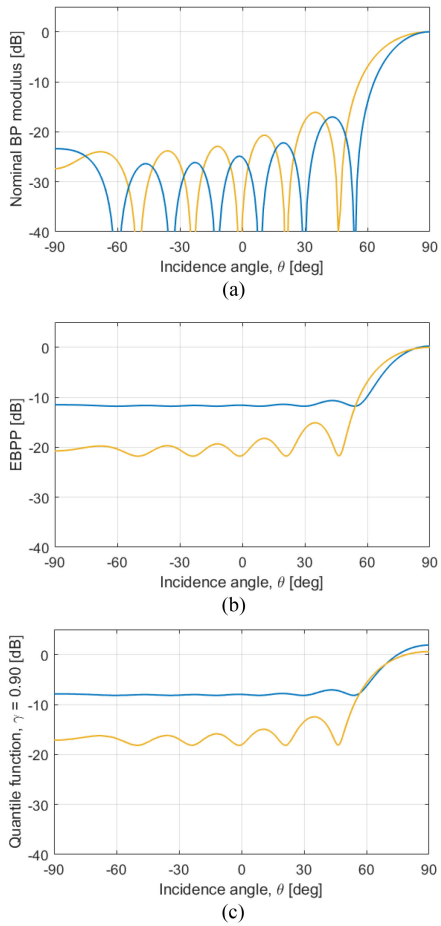

Fig. 10. Comparison of two weighting windows for the for C-3 arrays designed maximizing the directivity with: WNG ≥ -5 dB (blue); WNG ≥ 5 dB (golden). (a) NBPs. (b) EBPPs. (c) Quantile functions $\gamma = 0.90$.

with the two weighting windows are compared in Fig. 10(a): the NBP obtained with the lower bound set to -5 dB is definitely more directive, having narrower main-lobe and comparable side-lobe level. However, it is less robust to random errors than the NBP obtained with the lower-bound set to 5 dB. Conventionally, the impact of errors is assessed through the ABP mean power (frequently referred to as EBPP). Fig 10(b) compares the EBPPs for the two array designs and shows that the more robust design (WNG $\geq$ 5 dB) presents a noticeable lower side-lobe level, but its main-lobe width remains larger than that obtained by the less robust design (WNG ≥ -5 dB). While the less robust design seems to assure a better resolution, the more robust design seems to allow a better attenuation of interfering signals. When the quantile functions are inspected, the appraisal changes. Fig. 10(c) compares the two quantile functions with $\gamma = 0.90$. Recalling that the probability that the ABP modulus exceeds the quantile function, at each point of the horizontal axis, is $1{-}\gamma$, it is interesting to note that both the quantile functions cross the -3 dB level (which determines the main-lobe width) for θ close to 66°. Hence, the two designs have the same probability (specifically 10%) of exceeding such a level at about the same angle θ.

Recalling that the EBPP is very similar to the mean value of the ABP modulus (as observed in the previous subsection), one can conclude that, although the ABP modulus of the less robust design has, around $\theta = 66°$, a mean value lower than that of the more robust design, its variance is higher. It is evident that, to be effective, an array design procedure should consider not only the mean value of the ABP modulus (i.e., the EBPP), but also the variance. The quantile functions encompass all these aspects because they allow one to design superdirective BPs with a known (low) probability of exceeding a given profile. In this light, a design procedure which optimizes a given quantile function of the ABP modulus should be considered more meaningful than a procedure which optimizes the EBPP.

VI. Independence Between Side Lobes

The probability that the modulus of the ABP exceeds the quantile function $B_{q,\gamma}(\hat{\mathbf{u}})$ at a given direction $\hat{\mathbf{u}}$ is $(1 - \gamma)$. This property refers to a single point of the BP and does not provide any information on the statistical relationship between different BP points nor on the probability that the ABP exceeds the quantile function in more than one point. Main-lobe width (often measured at -3 dB) and side-lobe level are considered key performance in array systems that use beamforming as processing algorithm [1], [5], [12], [32], [34]. While the width of the main lobe is related to angular resolution, the level of the side lobes ensures the attenuation of signals coming from directions away from the steering direction. To obtain the expected attenuation, it is important to verify, in probabilistic terms, that no lobe exceeds the desired level over a significant angular interval. In fact, it is not the overrun of the desired level in single points that degrades significantly the performance, but rather the presence of even a single overrun that extends over a non-negligible size interval. Unfortunately, quantile functions do not provide *per se* any information on the number of overruns or their size.

To deepen this matter, as a first step, this section investigates the potential independence between the ABP at two arrival directions, namely $B(\hat{\mathbf{u}}_1)$ and $B(\hat{\mathbf{u}}_2)$. If the BP lobes are independent of each other, the statistical study of the overruns could be conducted focusing on individual lobes. Based on the conclusions reached in this section, the next section will propose an empirical approach to compute the probability of no overrun, with a size larger than a known value, of a given quantile function. Such a probability represents useful information in assessing the ability of a superdirective array to fulfill the task for which it was designed.

For notational simplicity, let us indicate $B(\hat{\mathbf{u}}_1)$ and $B(\hat{\mathbf{u}}_2)$ with B_1 and B_2, respectively, and let us define their real and imaginary parts as follows: $B_1 = B_{R_1} + jB_{I_1}$ and $B_2 = B_{R_2} + jB_{I_2}$. Moreover, let us define a two-dimensional complex random vector $\underline{\mathbf{b}} = [B_1, B_2]^T$, where ^{T} indicates the transpose.

B_1 and B_2 are independent complex RVs if the following three conditions are satisfied [41], [42]:

(j) $B_{R_1}, B_{I_1}, B_{R_2}, B_{I_2}$ are jointly Gaussian RVs;

(jj) all the entries of the complementary covariance matrix, $\mathbf{J}_{\underline{\mathbf{b}}\,\underline{\mathbf{b}}} = E\{\underline{\mathbf{b}}\,\underline{\mathbf{b}}^T\} - E\{\underline{\mathbf{b}}\}E\{\underline{\mathbf{b}}^T\}$, are equal to zero;

(jjj) the covariance matrix, $\mathbf{K}_{\underline{\mathbf{b}}\,\underline{\mathbf{b}}} = E\{\underline{\mathbf{b}}\,\underline{\mathbf{b}}^H\} - E\{\underline{\mathbf{b}}\}E\{\underline{\mathbf{b}}^H\}$, where ^{H} indicates the conjugate transpose, is diagonal.

Observing the definitions of B_R and B_I in (12) and (13), it is clear that every linear combination of $B_{R_1}, B_{I_1}, B_{R_2}, B_{I_2}$ results in the sum of *N* independent RVs. According to the central limit theorem, the PDF of the sum is approximately Gaussian. Therefore, for a number *N* sufficiently high, the condition (j) is satisfied.

$\mathbf{J}_{\underline{\mathbf{b}}\,\underline{\mathbf{b}}}$ is a 2 × 2 symmetric matrix (called also pseudo-covariance matrix) whose diagonal entries are

$$\mathbf{J}_{\underline{\mathbf{b}}\,\underline{\mathbf{b}}}[1,1] = \sigma^2_{R_1} - \sigma^2_{I_1} + j2\eta_{R_1,I_1} \tag{65}$$

$$\mathbf{J}_{\underline{\mathbf{b}}\,\underline{\mathbf{b}}}[2,2] = \sigma^2_{R_2} - \sigma^2_{I_2} + j2\eta_{R_2,I_2} \tag{66}$$

where $\sigma^2_{X_x}$ indicates the variance of B_{X_x} and η_{X_x,Y_y} indicates the covariance between B_{X_x} and B_{Y_y}. According to previous sections, B_{R_1} and B_{I_1} are almost independent variables with almost the same variance; the same holds for B_{R_2} and B_{I_2}. Therefore, $\mathbf{J}_{\underline{\mathbf{b}}\,\underline{\mathbf{b}}}[1,1]$ and $\mathbf{J}_{\underline{\mathbf{b}}\,\underline{\mathbf{b}}}[2,2]$ can be considered negligible. To satisfy the condition (jj), there remains to study whether the complementary covariance between B_1 and B_2,

$$\begin{aligned}\mathbf{J}_{\underline{\mathbf{b}}\,\underline{\mathbf{b}}}[1,2] = \mathbf{J}_{\underline{\mathbf{b}}\,\underline{\mathbf{b}}}[2,1] &= E\{B_1B_2\} - E\{B_1\}E\{B_2\} \\ &= \eta_{R_1,R_2} - \eta_{I_1,I_2} + j\left(\eta_{R_2,I_1} + \eta_{R_1,I_2}\right),\end{aligned} \tag{67}$$

is equal to zero or has a negligible modulus.

As $\mathbf{K}_{\underline{\mathbf{b}}\,\underline{\mathbf{b}}}$ is a 2×2 Hermitian matrix, to satisfy the condition (jjj), it is sufficient to study whether the covariance between B_1 and B_2,

$$\begin{aligned}\mathbf{K}_{\underline{\mathbf{b}}\,\underline{\mathbf{b}}}[1,2] = \mathbf{K}_{\underline{\mathbf{b}}\,\underline{\mathbf{b}}}[2,1]^* &= E\{B_1B_2^*\} - E\{B_1\}E\{B_2^*\} \\ &= \eta_{R_1,R_2} + \eta_{I_1,I_2} + j\left(\eta_{R_2,I_1} - \eta_{R_1,I_2}\right),\end{aligned} \tag{68}$$

is equal to zero or has a negligible modulus.

To assess the negligibility of the two covariances, $\mathbf{J}_{\underline{\mathbf{b}}\,\underline{\mathbf{b}}}[1,2]$ and $\mathbf{K}_{\underline{\mathbf{b}}\,\underline{\mathbf{b}}}[1,2]$, the related complex correlation coefficients [42]

$$\rho_{\mathbf{J}} = \frac{\mathbf{J}_{\underline{\mathbf{b}}\,\underline{\mathbf{b}}}[1,2]}{\sqrt{\sigma^2_{B_1}\sigma^2_{B_2}}} \tag{69}$$

$$\rho_{\mathbf{K}} = \frac{\mathbf{K}_{\underline{\mathbf{b}}\,\underline{\mathbf{b}}}[1,2]}{\sqrt{\sigma^2_{B_1}\sigma^2_{B_2}}}, \tag{70}$$

which satisfy $0 \le |\rho_{\mathbf{J}}| \le 1$ and $0 \le |\rho_{\mathbf{K}}| \le 1$, will be adopted. Assuming a spherical symmetry for the position errors, the ABP variance does not depend on the direction and, therefore, the denominators $\sqrt{\sigma^2_{B_1}\sigma^2_{B_2}}$ are simply equal to σ^2_B. Recalling (12) and (13), after some mathematics, it follows that

$$\begin{aligned}\eta_{R_1,R_2} = \frac{1}{2}\sum_{l=1}^{N}(\Lambda_l^n)^2 \Big[&\left(\overline{\Lambda}^2\mu_u^- - \overline{\Lambda}^2\mu^2_{\Theta}\right)\cos\left(\Phi^n_{l,1} - \Phi^n_{l,2}\right) \\ &+ \left(\overline{\Lambda}^2\mu_{2\varphi}\mu_u^+ - \overline{\Lambda}^2\mu^2_{\Theta}\right)\cos\left(\Phi^n_{l,1} + \Phi^n_{l,2}\right)\Big]\end{aligned} \tag{71}$$

$$\begin{aligned}\eta_{I_1,I_2} = \frac{1}{2}\sum_{l=1}^{N}(\Lambda_l^n)^2 \Big[&\left(\overline{\Lambda}^2\mu_u^- - \overline{\Lambda}^2\mu^2_{\Theta}\right)\cos\left(\Phi^n_{l,1} - \Phi^n_{l,2}\right) \\ &- \left(\overline{\Lambda}^2\mu_{2\varphi}\mu_u^+ - \overline{\Lambda}^2\mu^2_{\Theta}\right)\cos\left(\Phi^n_{l,1} + \Phi^n_{l,2}\right)\Big]\end{aligned} \tag{72}$$

$$\begin{aligned}\eta_{R_2,I_1} = \frac{1}{2}\sum_{l=1}^{N}(\Lambda_l^n)^2 \Big[&\left(\overline{\Lambda}^2\mu_u^- - \overline{\Lambda}^2\mu^2_{\Theta}\right)\sin\left(\Phi^n_{l,1} - \Phi^n_{l,2}\right) \\ &+ \left(\overline{\Lambda}^2\mu_{2\varphi}\mu_u^+ - \overline{\Lambda}^2\mu^2_{\Theta}\right)\sin\left(\Phi^n_{l,1} + \Phi^n_{l,2}\right)\Big]\end{aligned} \tag{73}$$

$$\begin{aligned}\eta_{R_1,I_2} = \frac{1}{2}\sum_{l=1}^{N}(\Lambda_l^n)^2 \Big[&-\left(\overline{\Lambda}^2\mu_u^- - \overline{\Lambda}^2\mu^2_{\Theta}\right)\sin\left(\Phi^n_{l,1} - \Phi^n_{l,2}\right) \\ &+ \left(\overline{\Lambda}^2\mu_{2\varphi}\mu_u^+ - \overline{\Lambda}^2\mu^2_{\Theta}\right)\sin\left(\Phi^n_{l,1} + \Phi^n_{l,2}\right)\Big]\end{aligned} \tag{74}$$

where the subscripts $_1$ and $_2$ used with the phases Φ_l^n indicate that they are computed according to (9), using $\hat{\mathbf{u}}_1$ and $\hat{\mathbf{u}}_2$ as argument, respectively. The new terms μ_u^-,μ_u^+,$\mu_{2\varphi}$ are defined as follows

$$\mu_{2\varphi} = E\{\cos(2\delta_{\varphi,l})\} \tag{75}$$

$$\mu_u^- = E\{\cos[k\boldsymbol{\varepsilon}_l \cdot (\hat{\mathbf{u}}_1 - \hat{\mathbf{u}}_2)]\} \tag{76}$$

$$\mu_u^+ = E\{\cos[k\boldsymbol{\varepsilon}_l \cdot (\hat{\mathbf{u}}_1 + \hat{\mathbf{u}}_2)]\} \tag{77}$$

Substituting the relation from (71) to (74) and the equations

$$\Phi^n_{l,1} - \Phi^n_{l,2} = k\mathbf{p}_l^n \cdot (\hat{\mathbf{u}}_1 - \hat{\mathbf{u}}_2) \tag{78}$$

$$\Phi^n_{l,1} + \Phi^n_{l,2} = 2(\varphi_l^n + \varphi_l^w) + k\mathbf{p}_l^n \cdot (\hat{\mathbf{u}}_1 + \hat{\mathbf{u}}_2 - 2\hat{\mathbf{u}}_0) \tag{79}$$

in (67) and (68), after some mathematics, one obtains, (80) shown at the bottom of the next page.

$$\rho_{\mathbf{K}} = \frac{\left(\overline{\Lambda}^2\mu_u^- - \overline{\Lambda}^2\mu^2_{\Theta}\right)\sum_{l=1}^{N}(\Lambda_l^n)^2\exp\{jk\mathbf{p}_l^n \cdot (\hat{\mathbf{u}}_1 - \hat{\mathbf{u}}_2)\}}{\left(\overline{\Lambda}^2 - \overline{\Lambda}^2\mu^2_{\Theta}\right)\sum_{l=1}^{N}(\Lambda_l^n)^2} \tag{81}$$

The term $\mu_{2\varphi}$, defined in (75) is present in the right-hand side of (50) and can be computed as in (55) or (58). To solve the expectation in μ_u^- and μ_u^+, position errors with zero-mean Gaussian PDF and variance σ^2_{ε} along the three axes can be assumed. In analogy with (52) and (54), one obtains

$$\mu_u^{\pm} = \exp\left(-\frac{k^2\sigma^2_{\varepsilon}\|\hat{\mathbf{u}}_1 \pm \hat{\mathbf{u}}_2\|^2}{2}\right) \tag{82}$$

where $\|\cdot\|^2$ represents the square norm of a vector. Because the nominal performance of a linear array placed on the *z*-axis does not depend on the azimuth angle α, one can assume that $\alpha_1 = \alpha_2$. In this case, the terms μ_u^- and μ_u^+ depend only on the difference between the broadside angles, θ_1 and θ_2, related to the directions $\hat{\mathbf{u}}_1$ and $\hat{\mathbf{u}}_2$, as follows

$$\mu_u^{\pm} = \exp\left\{-k^2\sigma^2_{\varepsilon}[1 \pm \cos(\theta_2 - \theta_1)]\right\} \tag{83}$$

A. Numerical Assessment

To assess the correlation between the BP lobes of a linear array, let us set θ_1 equal to the argument of the peak of a given lobe and assess the correlation coefficients for $\theta_2 = \theta$, $\theta \in$ [–90°, 90°]. Fig. 11 shows the profile of the absolute value of the correlation coefficient $\rho_{\mathbf{K}}$ for the array combinations C-2,

C-4, C-6 and C-8, in comparison with the related NBPs. In particular, for each array combination, the correlation coefficient is computed starting from the peak of the main lobe (i.e., $\theta_1 = 90°$) and from the peak of an arbitrarily chosen side lobe (i.e., $\theta_1 = -25°$, $-6°$, $-30°$ and $6°$ for C-2, C-4, C-6 and C-8, respectively). The complementary correlation coefficient $\rho_{\mathbf{J}}$ is not shown in Fig. 11 because in all the cases considered its absolute value is always very low, with a maximum equal to 0.05. Therefore, although not equal to zero, all the entries of the complementary covariance matrix are negligible and condition (jj) is almost satisfied.

Finally, the uncorrelatedness and independence of BP lobes principally depend on the profile of the correlation coefficient $\rho_{\mathbf{K}}$. From Fig. 11 one can observe that the correlation coefficient:

- remains high, close to one, within the lobe under examination;
- gradually decreases moving away from the lobe under examination, assuming an intermediate value (generally between 0.8 and 0.2) within the lobes adjacent to the one under examination;
- oscillates around low values (with a maximum of 0.26) within the lobes not adjacent to the one under examination.

Although there is no perfect uncorrelatedness between ABP points belonging to different NBP lobes, it can be concluded that their correlation is generally low, especially if the two lobes are far apart. Overall, although in previous studies focused on conventional arrays [25], [26] perfect independence between lobes was assumed, for superdirective arrays (with Gaussian, spherically symmetric position errors) it is possible to assume that non-adjacent lobes are almost independent, whereas adjacent lobes retain a significant correlation. The array combinations considered above are those for which the PDF set is S_2. If the PDF set S_1 is used in place of S_2, the profiles of the correlation coefficients change only marginally and the conclusions hold their validity.

VII. Overrun Size and Probability

In this section an empirical approach is adopted to investigate the size of the interval over which the ABP exceeds the quantile function $B_{q,\gamma}(\hat{\mathbf{u}})$, in relation with the probability $(1-\gamma)$ that a given point of such a quantile function is exceeded. The study is limited to the case of linear arrays with Gaussian, spherically symmetric position errors.

The following notations and conventions are introduced. For θ ranging from $-90°$ to $90°$, the NBP of a given array has a number T of lobes ($T-1$ side lobes and one main lobe), indicated as $\mathcal{L}_n,\ n = 1,\ \ldots,\ T$. The support of the lobe $\mathcal{L}_n$ is a finite interval of the θ-axis, (θ_s, θ_e), indicated as $\mathcal{I}_n$, whose size $(\theta_e - \theta_s)$ is indicated with $\mathcal{Z}_n$. An event in which the modulus of the ABP, $|B(\theta)|$, exceeds the quantile function $B_{q,\gamma}(\theta)$ over one or more sub-intervals of the region $\mathcal{I}_n$ is defined overrun of the lobe $\mathcal{L}_n$. If at least one of these sub-intervals has a size greater than a fraction $\Xi \in [0,\ 1]$, of the size $\mathcal{Z}_n$, then the event $\mathcal{OV}^n_{\gamma,\Xi}$ occurs. More precisely, for a given lobe n, a given probability γ, and a given fraction Ξ, the event $\mathcal{OV}^n_{\gamma,\Xi}$ occurs if the following condition is satisfied, one or more times:

$$|B(\theta)| > B_{q,\gamma}(\theta) \ \text{ for all } \theta \in (\theta_l, \theta_u)\,, \text{ where } \begin{cases} \theta_l \geq \theta_s \\ \theta_u \leq \theta_e \\ \frac{\theta_u - \theta_l}{\mathcal{Z}_n} > \Xi \end{cases} \tag{84}$$

Fig. 12 shows an overrun example for the C-5 array, in which the third lobe of the NBP (i.e., $\mathcal{L}_3$) has a support $\mathcal{I}_3$: (θ_s, θ_e), with $\theta_s = -10°, \theta_e = 32°$, and the size $\mathcal{Z}_3$ equal to 42°. The plot shows an ABP that exceeds the quantile function $B_{q,0.90}(\theta)$ for all $\theta \in$ (1.5°, 24.5°), producing an overrun whose size is 23°. Because 23°/42° is 0.55, the event $\mathcal{OV}^3_{0.90,\Xi}$ occurs for all $\Xi \in [0,\ 0.55)$.

Here the aim is to assess the probability that the event $\mathcal{OV}^n_{\gamma,\Xi}$ does not occur, i.e., the probability that none of the overruns (if any) of the lobe $\mathcal{L}_n$ has a size larger than $\Xi\mathcal{Z}_n$. This probability, as a function of Ξ, is indicated by $\mathrm{C}^n_\gamma(\Xi)$ and is defined as follows

$$\mathrm{C}^n_\gamma\ (\Xi) = \ 1 - \Pr\left(\mathcal{OV}^n_{\gamma,\Xi}\right) \tag{85}$$

where Pr(a) is the probability of the event a.

For each combination in Table I, 10^4 independent realizations of the ABP were computed and the $\Pr(\mathcal{OV}^n_{\gamma,\Xi})$ was estimated through the relative frequency of the event. The relative frequency was computed as a function of Ξ and for every lobe of the superdirective NBP, including the main-lobe. The number of lobes was: $T = 3$ for C-1 and C-2; $T = 7$ for C-3 and C-4; $T = 4$ for C-5 and C-6; $T = 12$ for C-7 and C-8. This study was repeated for two values of the probability γ, i.e., the variable used to identify the quantile function $B_{q,\gamma}(\hat{\mathbf{u}})$: $\gamma = 0.90$ and $\gamma = 0.99$. The corresponding functions $\mathrm{C}^n_\gamma(\Xi)$, for $n = 1,\ \ldots, T$, are shown in Fig. 13. Each panel contains a number of curves equal to the number of lobes, T, present in the NBP. One can observe that most of these curves cross the probability level $\mathrm{C}^n_\gamma = \gamma$ for $\Xi \in [0.4,\ 0.5]$. Consequently, for $0.9 \leq \gamma \leq 1$, the following empirical relation can be deduced

$$\mathrm{C}^n_\gamma\,(0.45) \approx \gamma \tag{86}$$

for whatever n, $n = 1,\ \ldots, T$. This means that, when only the support of the n-th lobe of the NBP is considered, the probability that the ABP does not show any overrun of the quantile function $B_{q,\gamma}(\theta)$ with a size larger than 0.45 $\mathcal{Z}_n$ is approximately equal to γ.

Although adjacent lobes retain significant correlation, it is possible to assume the BP lobes to be independent (as is mostly the case for non-adjacent lobes), evaluating *a posteriori* the errors introduced by this choice. Assuming the independence, the property in (86) can be used to approximate the probability

$$\rho_{\mathbf{J}} = \frac{\left(\overline{\Lambda}^2 \mu_{2\varphi} \mu_u^+ - \overline{\Lambda}^2 \mu_\Theta^2\right) \sum_{l=1}^N \left(\Lambda_l^n\right)^2 \exp\left\{j\left[2\left(\varphi_l^n + \varphi_l^w\right) + k\mathbf{p}_l^n \cdot \left(\hat{\mathbf{u}}_1 + \hat{\mathbf{u}}_2 - 2\hat{\mathbf{u}}_0\right)\right]\right\}}{\left(\overline{\Lambda}^2 - \overline{\Lambda}^2 \mu_\Theta^2\right) \sum_{l=1}^N \left(\Lambda_l^n\right)^2} \tag{80}$$

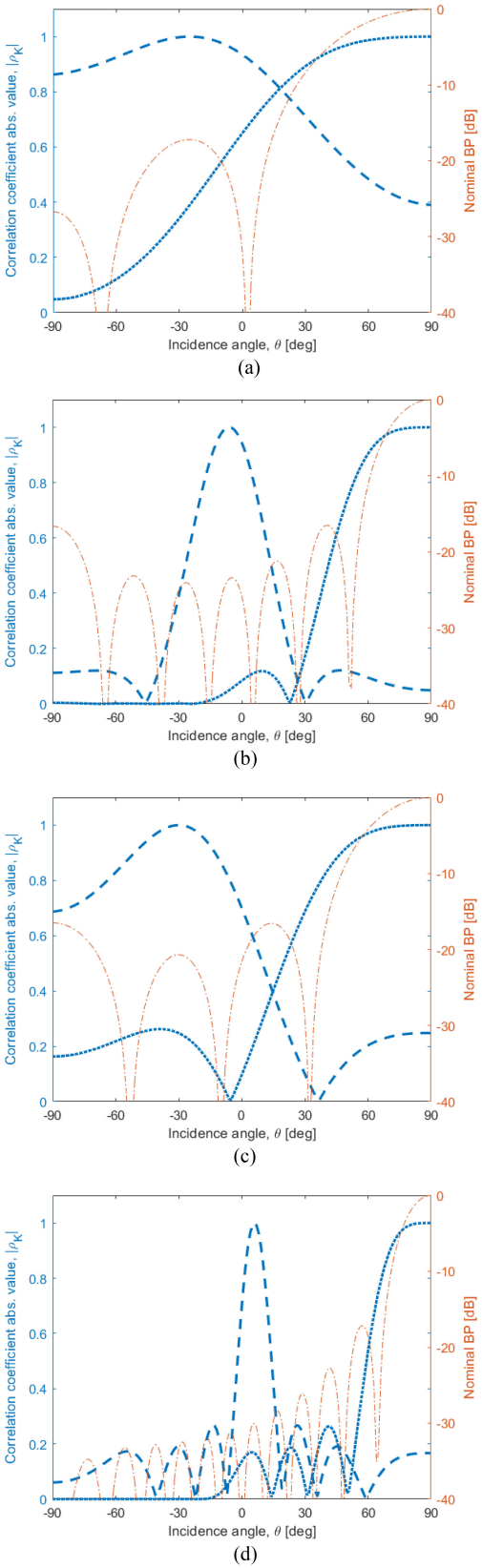

Fig. 11. Absolute value of the correlation coefficient $\rho_{\mathbf{K}}$ for $\theta_2 = \theta$, $\theta \in [-90°, 90°]$, in relation with the NBP (dash-dotted). (a) C-2: $\theta_1 = 90°$ (dotted); $\theta_1 = -25°$ (dashed). (b) C-4: $\theta_1 = 90°$ (dotted); $\theta_1 = -6°$ (dashed). (c) C-6: $\theta_1 = 90°$ (dotted); $\theta_1 = -30°$ (dashed). (d) C-8: $\theta_1 = 90°$ (dotted); $\theta_1 = 6°$ (dashed).

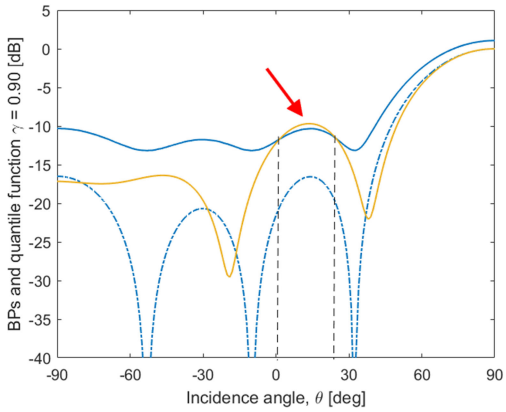

Fig. 12. NBP (blue dash-dotted line) for the C-5 array with the related quantile function $\gamma = 0.90$ (blue solid line). The red arrow indicates the overrun of the quantile function by the modulus of an ABP (golden line). The overrun support is (1.5°, 24.5°).

TABLE IV
COMPARISON OF THE APPROXIMATION γ^T FOR THE PROBABILITY THAT THE ABP DOES NOT SHOW ANY OVERRUN OF THE QUANTILE FUNCTION $B_{q,\gamma}(\theta)$, WITH A SIZE EXCEEDING $0.45\pi/T$ (T BEING THE NUMBER OF LOBES IN THE NBP), WITH THE EXPERIMENTAL ESTIMATION OF THE SAME PROBABILITY

Comb.	T	$\mathcal{I}$ [deg]	$\gamma = 0.90$		$\gamma = 0.99$	
			γ^T	Est. $\tilde{\mathrm{C}}_\gamma(\mathcal{I})$	γ^T	Est. $\tilde{\mathrm{C}}_\gamma(\mathcal{I})$
C-1	3	27.0°	0.729	0.743	0.970	0.972
C-2	3	27.0°	0.729	0.748	0.970	0.971
C-3	7	11.6°	0.478	0.467	0.932	0.929
C-4	7	11.6°	0.478	0.494	0.932	0.929
C-5	4	20.3°	0.656	0.633	0.961	0.958
C-6	4	20.3°	0.656	0.651	0.961	0.958
C-7	12	6.8°	0.282	0.276	0.886	0.881
C-8	12	6.8°	0.282	0.285	0.886	0.880

that the entire ABP does not show any overrun exceeding a given size. Since the average lobe size is equal to π/T [rad], the probability $\tilde{\mathrm{C}}_\gamma(\mathcal{I})$ that the modulus of the ABP, $|B(\theta)|$, does not show any overrun of the quantile function $B_{q,\gamma}(\theta)$ with a size larger than $\mathcal{I}$, $\mathcal{I} = 0.45\,\pi/T$ [rad], can be approximated as follows:

$$\tilde{\mathrm{C}}_\gamma(\mathcal{I}) \approx \gamma^T. \tag{87}$$

This equation needs to be carefully assessed, especially to appraise the magnitude of the errors introduced by the independence assumption.

A. Numerical Assessment

To evaluate the precision of the proposed approximation, $5 \cdot 10^4$ independent realizations of the ABP were computed for each combination in Table I and the probability $\tilde{\mathrm{C}}_\gamma(\mathcal{I})$ was estimated through the relative frequency, for $\gamma = 0.90$ and $\gamma = 0.99$. The estimated value of $\tilde{\mathrm{C}}_\gamma(\mathcal{I})$ was compared with γ^T and the related results were reported in Table IV. The absolute value of the difference between the approximated computation and the experimental estimation of $\tilde{\mathrm{C}}_\gamma(\mathcal{I})$ is often below 0.01, with a maximum of 0.023. This confirms that: for $0.9 \leq \gamma \leq 1$, γ^T represents a good approximation of the probability that there

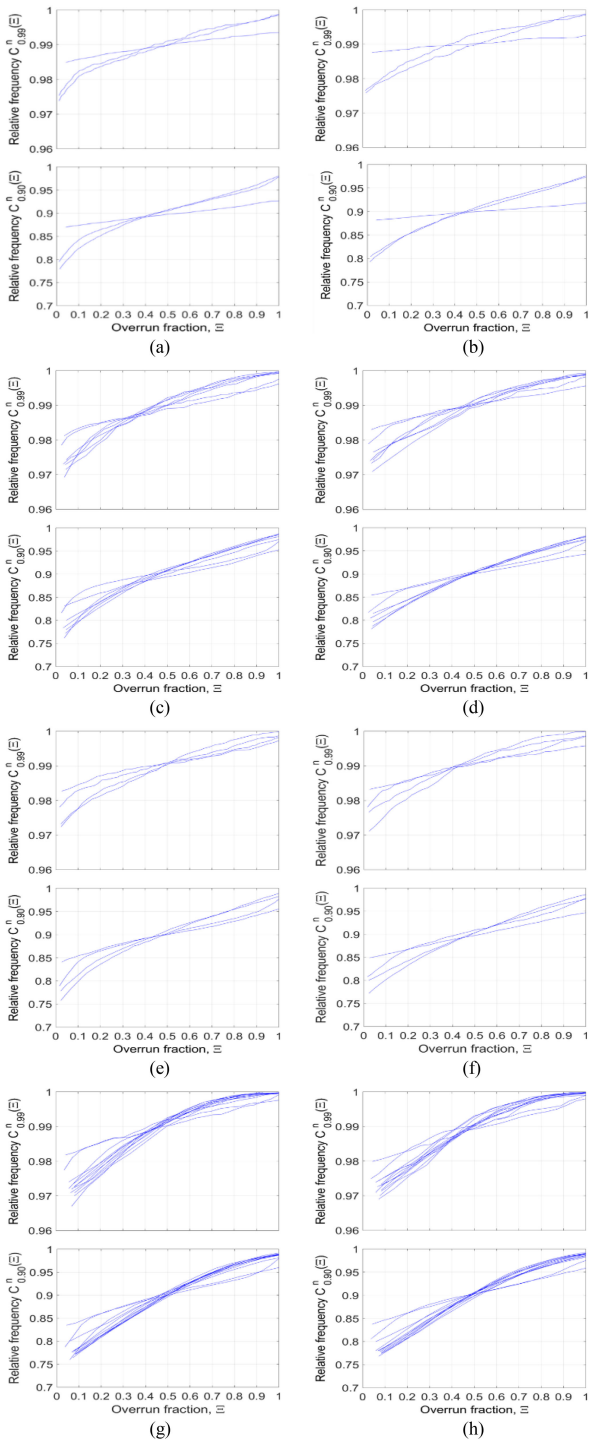

Fig. 13. Probability that none of the overruns of the quantile function $B_{q,\gamma}(\theta)$, for a given lobe of the NBP, has a size larger than a fraction Ξ of the lobe support. The study is repeated for each lobe, for $\gamma = 0.90$ and $\gamma = 0.99$. (a) C-1; (b) C-2; (c) C-3; (d) C-4; (e) C-5; (f) C-6; (g) C-7; (h) C-8.

is no overrun, with size larger than $0.45\,\pi/T$ [rad], of the quantile function $B_{q,\gamma}(\theta)$; the correlation present between adjacent lobes did not introduce significant errors when the independence was assumed to derive (87) from (86). Finally, it is important to recall that the array and error characteristics from which this relation was empirically derived are those listed in Table I.

VIII. Conclusion

Using the Rician PDF to approximate the statistics of the ABP modulus requires verifying the negligibility of two terms that measure the difference between the variances of the ABP real and imaginary parts and the correlation coefficient between these two parts. Similarly, the independence between different BP lobes requires verifying the profile of two correlation coefficients as a function of the arrival direction. In the latter case, it was necessary to assume spherical symmetry for the statistics of the position errors to achieve a compact expression.

Linear superdirective arrays with end-fire steering and a number of elements high enough to apply the central limit theorem show a remarkable adherence to the Rician PDF and a partial independence between the lobes, especially non-adjacent ones. These two achievements form the basis for identifying the quantile BP functions (i.e., functions with a known probability of being exceeded by the ABP, at any direction) and for calculating the probability that no overrun occurs with a support larger than a given value. For the linear end-fire arrays examined, an empirical equation for calculating this probability was proposed and experimentally assessed.

The new knowledge and mathematical tools introduced in this study allow, on the one hand, to repeat the investigation on ABP Ricianity, lobes' independence and probability of extended overruns for other array geometries and characteristics, on the other hand, to hypothesize a new class of methods for the design of superdirective arrays, aimed at the optimization of the quantile BP functions. The meaning of the latter is indeed more consistent with the goal of robust design than that of the EBPP, used in many literature methods.

Appendix A
Proof of Proposition 1

Recalling *Assumptions 1* and *2* and adopting the notation in (22), the term Θ_1^R in (17) can be rewritten as

$$\Theta_1^R = \overline{\Lambda}^2 \sum_{l=1}^{N} (\Lambda_l^n)^2 \left[\frac{1}{2} + \frac{1}{2} E\left\{\cos\left(2\Phi_l^n + 2\Phi_l\right)\right\}\right] \tag{88}$$

The expectation can be developed as follows

$$E\left\{\cos\left(2\Phi_l^n + 2\Phi_l\right)\right\} = \cos\left(2\Phi_l^n\right) E\left\{\cos\left(2\Phi_l\right)\right\} - \sin\left(2\Phi_l^n\right) E\left\{\sin\left(2\Phi_l\right)\right\} \tag{89}$$

and, applying (10) and *Assumption 3*, it is straightforward to show that

$$E\left\{\cos\left(2\Phi_l\right)\right\} = E\left\{\cos\left(2\delta_{\varphi,l}\right)\right\} E\left\{\cos\left(2k\boldsymbol{\varepsilon}_l \cdot \hat{\mathbf{u}}\right)\right\} \tag{90}$$

and

$$E\left\{\sin\left(2\Phi_l\right)\right\} = 0 \tag{91}$$

Because under *Assumption 1* the expectations in (90) do not depend on l, introducing the notation in (24) the expectation in (89) can finally be rewritten as

$$E\left\{\cos\left(2\Phi_l^n + 2\Phi_l\right)\right\} = \cos\left(2\Phi_l^n\right) \mu_{2\Theta} \tag{92}$$

Substituting this result in (88), equation (19) is easily obtained.

Recalling *Assumptions 1* and *2* and adopting the notation in (21), the term Θ_2^R in (18) can be rewritten as

$$\Theta_2^R = \overline{\Lambda}^2 \sum_{l=1}^{N} \sum_{m=1,m\neq l}^{N} \Lambda_l^n \Lambda_m^n E\left\{\cos\left(\Phi_l^n+\Phi_l\right)\right\} E\left\{\cos\left(\Phi_m^n+\Phi_m\right)\right\} \tag{93}$$

In analogy with the above

$$E\left\{\cos\left(\Phi_l^n+\Phi_l\right)\right\} = \cos\left(\Phi_l^n\right) E\left\{\cos\left(\Phi_l\right)\right\} - \sin\left(\Phi_l^n\right) E\left\{\sin\left(\Phi_l\right)\right\} \tag{94}$$

$$E\left\{\cos\left(\Phi_l\right)\right\} = E\left\{\cos\left(\delta_{\varphi,l}\right)\right\} E\left\{\cos\left(k\boldsymbol{\varepsilon}_l \cdot \hat{\mathbf{u}}\right)\right\} \tag{95}$$

and $E\{\sin(\Phi_l)\} = 0$. Because under *Assumption 1* the expectations in (95) do not depend on *l*, introducing the notation in (23) the expectation in (94) can be rewritten as

$$E\left\{\cos\left(\Phi_l^n+\Phi_l\right)\right\} = \cos\left(\Phi_l^n\right) \mu_\Theta \tag{96}$$

Obviously, the same reasoning can be applied to the expectation with index *m*. Substituting the results in (90), equation (20) is easily obtained.

Appendix B
Proof of Proposition 2

From (12) and (13) the term $E\{B_R B_I\}$ can be written as

$$\begin{aligned} &E\left\{B_R B_I\right\} \\ &= E\left\{\sum_{l=1}^{N}\sum_{m=1}^{N} \Lambda_l^n \Lambda_m^n \Lambda_l \Lambda_m \cos\left(\Phi_l^n+\Phi_l\right) \sin\left(\Phi_m^n+\Phi_m\right)\right\} \\ &= \Theta_1^\eta + \Theta_2^\eta \end{aligned} \tag{97}$$

where

$$\Theta_1^\eta = E\left\{\sum_{l=1}^{N} \left(\Lambda_l^n\right)^2 \Lambda_l^2 \cos\left(\Phi_l^n+\Phi_l\right) \sin\left(\Phi_l^n+\Phi_l\right)\right\} \tag{98}$$

$$\Theta_2^\eta = E\left\{\sum_{l=1}^{N}\sum_{m=1,m\neq l}^{N} \Lambda_l^n \Lambda_m^n \Lambda_l \Lambda_m \cos\left(\Phi_l^n+\Phi_l\right) \cdot \sin\left(\Phi_m^n+\Phi_m\right)\right\} \tag{99}$$

Recalling that under *Assumption 3* $E\{\sin(\Phi_l)\} = E\{\sin(2\Phi_l)\} = 0$, applying *Assumptions 1* and *2* and the notation in (23) and (24), it is possible to obtain the following relations

$$\begin{aligned} &E\left\{\cos\left(\Phi_l^n+\Phi_l\right) \sin\left(\Phi_l^n+\Phi_l\right)\right\} \\ &= \frac{1}{2} E\left\{\sin\left(2\Phi_l^n+2\Phi_l\right)\right\} = \frac{1}{2} \sin\left(2\Phi_l^n\right) \mu_{2\Theta} \end{aligned} \tag{100}$$

$$\begin{aligned} &E\left\{\cos\left(\Phi_l^n+\Phi_l\right) \sin\left(\Phi_m^n+\Phi_m\right)\right\} \\ &= E\left\{\cos\left(\Phi_l^n+\Phi_l\right)\right\} E\left\{\sin\left(\Phi_m^n+\Phi_m\right)\right\} \\ &= \mu_\Theta^2 \cos\left(\Phi_l^n\right) \sin\left(\Phi_m^n\right) \end{aligned} \tag{101}$$

Adopting the notation in (21) and (22) and the results in (100) and (101), under *Assumptions 1* and *2*, (98) and (99) can be rewritten as in (37) and (38), respectively.

Recalling that the variance is $\eta_{R,I} = E\{B_R B_I\} - \overline{B}_R \overline{B}_I$, through (97), (28) and (29), it can be written as

$$\eta_{R,I} = \Theta_1^\eta + \Theta_2^\eta - \overline{\Lambda}^2 \mu_\Theta^2 \sum_{l=1}^{N}\sum_{m=1}^{N} \Lambda_l^n \Lambda_m^n \cos\Phi_l^n \sin\Phi_m^n \tag{102}$$

Substituting (37) and (38) in this equation and reorganizing the terms, it is easy to obtain the expression in (39).

Appendix C
Details on Spherical Symmetry of Position Errors

To investigate spherical symmetry, it is convenient to rewrite the vectors $\hat{\mathbf{u}}$ and $\boldsymbol{\varepsilon}_l$ in a new coordinate system, centered on $\mathbf{p}_l^n$, with the z-axis parallel to $\hat{\mathbf{u}}$. In the new coordinate system

$$\hat{\mathbf{u}} = [0,0,1]\,; \boldsymbol{\varepsilon}_l = r_l \left[\sin\tilde{\chi}_l \cos\tilde{\alpha}_l, \sin\tilde{\chi}_l \sin\tilde{\alpha}_l, \cos\tilde{\chi}_l\right] \tag{103}$$

where r_l is modulus of the displacement vector $\boldsymbol{\varepsilon}_l$, $\tilde{\alpha}_l$ and $\tilde{\chi}_l$ are the azimuth and polar angles, respectively, that identify the direction of $\boldsymbol{\varepsilon}_l$ in the new coordinate system. According to *Assumptions 1* and *2*, r_l, $\tilde{\alpha}_l$ and $\tilde{\chi}_l$ are independent RVs and their PDFs do not depend on *l*. The spherical symmetry is obtained by setting a uniform density for $\tilde{\alpha}$ and $\tilde{\chi}$. In spherical coordinates, this means that

$$\beta_{\tilde{\alpha},\tilde{\chi}}\left(\tilde{\alpha},\tilde{\chi}\right) = \beta_{\tilde{\alpha}}\left(\tilde{\alpha}\right) \beta_{\tilde{\chi}}\left(\tilde{\chi}\right) = \frac{\sin\tilde{\chi}}{4\pi}, \tilde{\alpha} \in [-\pi,\pi]\,, \tilde{\chi} \in [0,\pi] \tag{104}$$

In these conditions, the expectation in (59) results to be

$$\begin{aligned} &E\left\{\cos\left(k\boldsymbol{\varepsilon}_l \cdot \hat{\mathbf{u}}\right)\right\} \\ &= \frac{1}{4\pi} \int_0^\infty \int_{-\pi}^{\pi} \int_0^{\pi} \cos\left(kr\cos\tilde{\chi}\right) \sin\tilde{\chi} \beta_r\left(r\right) d\tilde{\chi} d\tilde{\alpha} dr \\ &= \int_0^\infty \operatorname{sinc}\left(\frac{kr}{\pi}\right) \beta_r\left(r\right) dr \end{aligned} \tag{105}$$

where $\beta_r(r)$ is the PDF of the modulus of the error vector.

References

[1] H. L. Van Trees, *Optimum Array Processing, Part IV of Detection, Estimation, and Modulation Theory*. New York, NY, USA: Wiley, 2002.

[2] S. A. Schelkunoff, "A mathematical theory of linear arrays," *Bell Syst. Tech. J.*, vol. 22, pp. 80–107, Jan. 1943.

[3] E. N. Gilbert and S. P. Morgan, "Optimum design of directive antenna arrays subject to random variations," *Bell Syst. Tech. J.*, vol. 34, pp. 637–663, May 1955.

[4] H. Cox, R. Zeskind, and T. Kooij, "Practical supergain," *IEEE Trans. Acoust., Speech, Signal Process.*, vol. ASSP-34, no. 3, pp. 393–398, Jun. 1986.

[5] R. C. Hansen, *Phased Array Antennas*, 2nd ed. Hoboken, NJ, USA: Wiley, 2009.

[6] R. C. Hansen, *Electrically Small, Superdirective and Superconducting Antennas*. New York, NY, USA: Wiley, 2006.

[7] F. Traverso, M. Crocco, and A. Trucco, "Design of frequency-invariant robust beam patterns by the oversteering of end-fire arrays," *Signal Process.*, vol. 99, pp. 129–135, Jun. 2014.
[8] X. Wang, I. Cohen, J. Chen, and J. Benesty, "On robust and high directive beamforming with small-spacing microphone arrays for scattered sources," *IEEE/ACM Trans. Audio, Speech, Lang. Process.*, vol. 27, no. 4, pp. 842–852, Apr. 2019.
[9] A. Debard, A. Clemente, C. Delaveaud, P. Potier, and P. Pouliguen, "Limitations and optimization of supergain end-fire arrays," in *Proc. 13th Europ. Conf. Antennas Propag.*, Krakow, Poland, 2019, pp. 1–4.
[10] P. Hazdra, J. Kracek, and T. Lonsky, "On end-fire super directivity of arrays of two elementary dipoles and isotropic radiators," *IET Microw. Antennas Propag.*, vol. 13, no. 14, pp. 2405–2411, 2019.
[11] A. Vallecchi, A. Radkovskaya, L. Li, G. Faulkner, C. J. Stevens, and E. Shamonina, "Superdirective dimers of coupled self-resonant split ring resonators: Analytical modelling and numerical and experimental validation," *Sci. Rep.*, vol. 10, 2020, Paper 274.
[12] J. Bitzer and K. U. Simmer, "Superdirective microphone arrays," in *Microphone Arrays: Signal Processing Techniques and Applications*, M. S. Brandstein and D. B. Ward, Eds. New York, NY, USA: Springer-Verlag, 2001, pp. 19–38.
[13] G. Huang, J. Chen, and J. Benesty, "A flexible high directivity beamformer with spherical microphone arrays," *J. Acoustic. Soc. Amer.*, vol. 143, pp. 3024–3035, May 2018.
[14] M. Siderius, "Using practical supergain for passive imaging with noise," *J. Acoustic. Soc. Amer.*, vol. 131, pp. EL14–EL20, Jan. 2012.
[15] A. Trucco, S. Martelli, and M. Crocco, "Low-cost acoustic cameras for underwater wideband passive imaging," *IEEE J. Ocean. Eng.*, vol. 40, no. 4, pp. 929–937, Oct. 2015.
[16] D. P. Scholnik and J. O. Coleman, "Superdirectivity and SNR constraints in wideband array-pattern design," in *Proc. IEEE Int. Radar Conf.*, Atlanta, GA, USA, 2001, pp. 181–186.
[17] S. Mikki, S. Clauzier, and Y. Antar, "A correlation theory of antenna directivity with applications to superdirective arrays," *IEEE Antennas Wireless Propag. Lett.*, vol. 18, no. 5, pp. 811–815, May 2019.
[18] S. Doclo and M. Moonen, "Design of broadband beamformers robust against gain and phase errors in the microphone array characteristics," *IEEE Trans. Signal Process.*, vol. 51, no. 10, pp. 2511–2526, Oct. 2003.
[19] S. Doclo and M. Moonen, "Superdirective beamforming robust against microphone mismatch," *IEEE Trans. Audio, Speech, Lang. Process.*, vol. 15, no. 2, pp. 617–631, Feb. 2007.
[20] H. Chen and W. Ser, "Design of robust broadband beamformers with passband shaping characteristics using Tikhonov regularization," *IEEE Trans. Audio, Speech, Lang. Process.*, vol. 17, no. 4, pp. 665–681, May 2009.
[21] M. Crocco and A. Trucco, "Design of robust superdirective arrays with a tunable tradeoff between directivity and frequency-invariance," *IEEE Trans. Signal Process.*, vol. 59, no. 5, pp. 2169–2181, May 2011.
[22] A. Trucco and M. Crocco, "Design of an optimum superdirective beamformer through generalized directivity maximization," *IEEE Trans. Signal Process.*, vol. 62, no. 23, pp. 6118–6129, Dec. 2014.
[23] J. Ruze, "The effect of aperture errors on the antenna radiation pattern," *Nuovo Cimento (Suppl.)*, vol. 9, pp. 364–380, Mar. 1952.
[24] R. Elliott, "Mechanical and electrical tolerances for two-dimensional scanning antenna arrays," *IRE Trans. Antennas Propag.*, vol. 6, pp. 114–120, Jan. 1958.
[25] L. Rondinelli, "Effects of random errors on the performance of antenna arrays of many elements," in *Proc. IRE Int. Conv. Rec.*, New York, NY, USA, 1959, pp. 174–189.
[26] J. L. Allen, "The theory of array antennas (with emphasis on radar applications)," Mass. Inst. of Tech., Lincoln Lab., Lexington, MA, USA, Tech. Rep. 323, Jul. 1963.
[27] J. L. Brown, Jr., "Variation of array performance with respect to statistical phase fluctuations," *J. Acoustic. Soc. Amer.*, vol. 34, pp. 1927–1928, Dec. 1962.
[28] J. Howard, "Statistical patterns of a general array," *IEEE Trans. Antennas Propag.*, vol. ASSP-15, no. 1, pp. 60–65, Jan. 1967.
[29] D. J. Ramsdale and R. A. Howerton, "Effect of element failure and random errors in amplitude and phase on the sidelobe level attainable with a linear array," *J. Acoustic. Soc. Amer.*, vol. 68, pp. 901–906, Sep. 1980.
[30] J. K. Hsiao, "Design of error tolerance of a phased array," *Electron. Lett.*, vol. 21, pp. 834–836, Sep. 1985.
[31] P. D. Kaplan, "Predicting antenna sidelobe performance," The Mitre Corp., Bedford, MA, USA, Tech. Rep. ESD-TR-86-234, Aug. 1986.
[32] R. O. Nielsen, *Sonar Signal Processing*, Boston, MA, USA: Artech House, 1991.
[33] Y. S. Shifrin and L. G. Kornienko, "The state-of-the-art of the statistical theory of antenna arrays," in *Proc. 6th Int. Symp. Antennas, Prop. EM Theory*, Beijing, China, Oct. 2003, pp. 176–181.
[34] R. J. Mailloux, *Phased Array Antenna Handbook*, 2nd ed. Boston, MA, USA: Artech House, 2005.
[35] M. K. Simon, *Probability Distributions Involving Gaussian Random Variables: A Handbook for Engineers and Scientists*. New York, NY, USA: Springer Science & Business Media, 2007.
[36] A. Papoulis and S. U. Pillai, *Probability, Random Variables and Stochastic Processes*, 4th ed. New York, NY, USA: McGraw-Hill, 2015.
[37] M. R. Spiegel, S. Lipschutz, and J. Liu, *Mathematical Handbook of Formulas and Tables*, 4th ed. New York, NY, USA: McGraw-Hill, 2012.
[38] H. Cox, R. M. Zeskind, and M. M. Owen, "Robust adaptive beamforming," *IEEE Trans. Acoust. Speech Signal Process.*, vol. ASSP-35, no. 10, pp. 1365–1376, Oct. 1987.
[39] J. Li, P. Stoica, and Z. Wang, "Doubly constrained robust capon beamforming," *IEEE Trans. Signal Process.*, vol. 52, no. 9, pp. 2407–2423, Sep. 2004.
[40] S. Yan and Y. Ma, "Robust supergain beamforming for circular array via second-order cone programming," *Appl. Acoust.*, vol. 66, pp. 1018–1032, 2005.
[41] S. M. Kay, *Fundamentals of Statistical Signal Processing: Estimation Theory*. Upper Saddle River, NJ, USA: Prentice-Hall, 1993.
[42] T. Adali and P. J. Schreier, "Optimization and estimation of complex-valued signals: Theory and applications in filtering and blind source separation," *IEEE Signal Process. Mag.*, vol. 31, no. 5, pp. 112–128, Sep. 2014.

Andrea Trucco (Senior Member, IEEE) was born in Genoa, Italy, on February 10, 1970. He received the M.Sc. and Ph.D. degrees in electronic and computer engineering from the University of Genoa, Genoa, Italy, in 1994 and 1998, respectively. Since 1999, he has been with the University of Genoa, where he was appointed as a Professor of Telecommunications in 2016. He was the Vice-Rector for International Relations during 2015–2020 and Vice-Director of the Department of Biophysical and Electronic Engineering during 2008–2012. He was also a Senior Researcher with the Italian Institute of Technology during 2011–2015. He was the Principal Investigator in many research projects, funded by the EU, national agencies and industrial companies. He is the author of more than 200 scientific papers (90 in international journals) and inventor in seven international patents. His research interests include acoustics, signal processing, pattern recognition, sonar systems, medical ultrasound, and fault diagnosis. He is also an Associate Editor for the IEEE JOURNAL OF OCEANIC ENGINEERING and IEEE TRANSACTIONS ON ULTRASONICS, FERROELECTRICS, AND FREQUENCY CONTROL. He won the student paper competitions organized by the 9th International Symposium Unmanned Untethered Submersible Technology 1995 and MTS/IEEE Oceans '97 International Conference 1997.